Spatial risk assessment of social vulnerability to contaminated river water
A case study of Coosa River watershed

by

Al Artat Bin Ali

A thesis submitted to the Graduate Faculty of
Auburn University in partial fulfillment of the
requirements for the Degree of
Master of Science

Auburn, Alabama

August 3, 2024

Keywords: Social Vulnerability, likelihood of Contamination with Flood Risk, Multi-Criteria Decision Analysis, Toxic Release Inventory

Committee Members

Dr. Jake R. Nelson, Chair, Assistant Professor, Department of Geosciences

Dr. Stephanie R. Rogers, Assistant Professor, Department of Geosciences

Dr. Evaden F. Brantley, Professor, Department of Crop, Soil & Environmental Sciences

Abstract

This study investigates the spatiotemporal patterns of toxic release inventory (TRI) releases within the Coosa River watershed and the compounded hazards of flooding and industrial emissions through a spatial risk assessment framework, focusing on social vulnerability to contaminated floodwaters and emphasizing the impacts on low-income and racially diverse communities. By integrating socio-economic indicators, flood risk factors, and TRI chemical release data from 2000, 2010, and 2020, the research employs Multi-Criteria Decision Analysis (MCDA), specifically the Analytic Hierarchy Process (AHP), to identify areas where socially vulnerable communities are at risk of contamination associated with flood risk. The findings reveal a prominent increase in chemical discharges to water despite an overall reduction in discharges to land, water, and air, highlighting risk to vulnerable populations. The analysis shows shifts over time in the location and extent of pollution as well as high and low flood potential areas, demonstrating how changing socio-economic conditions have influenced community susceptibility to flooding and contamination. This integrative approach offers a comprehensive environmental risk assessment and underscores the importance of adaptive and effective risk management strategies to address the dynamic interactions between flooding, industrial activities, and socio-economic conditions.

Acknowledgement

I am deeply grateful to my family for their unwavering support throughout my academic journey. My heartfelt gratitude goes especially to my wife, Sharmin Sultana Toa, and my son, Al Arshan Bin Artat, who moved to Auburn with me, making significant sacrifices by leaving everything behind in Bangladesh to support me. Your love and understanding have been my greatest strength. To my parents, your endless encouragement, belief in my potential, and countless sacrifices have been the foundation of my achievements. Your support has been the driving force behind my success, and I cannot thank you enough for everything you have done for me. I am also deeply appreciative of my dear friends whose support and encouragement have been invaluable. A special thanks to my lab mates, SK Nafiz Rahaman, Dikshya Panta, and Ansleigh Bright. Your willingness to help and the memorable moments we shared have enriched this journey. Finally, I wish to express my deepest gratitude to my advisor, Dr. Jake Nelson. As an international graduate student, navigating this path would have been exceedingly difficult for me without your expert guidance, mentorship, understanding, and patience. Your support has been invaluable and has made my academic journey truly enjoyable. Thank you all for being an integral part of my journey.

Table of Contents

List of Tables

List of Figures

List of Abbreviations

ADEM	Alabama Department of Environmental Management
AHP	Analytic Hierarchy Process
DEM	Digital Elevation Model
EPA	Environmental Protection Agency
IPUMS	Integrated Public Use Microdata Series
MCDA	Multi-Criteria Decision Analysis
NHGIS	National Historical Geographic Information System
NDVI	Normalized Difference Vegetation Index
PCA	Principal Component Analysis
SoVI	Social Vulnerability Index
TMLDs	Total Maximum Daily Loads
TWI	Topographic Wetness Index
TRI	Toxic Release Inventory
US EPA	United States Environmental Protection Agency
USGS	United States Geological Survey

1. Introduction:

Water-related disasters, arising from both natural and anthropogenic hazards, represent some of the most critical environmental challenges of our time, posing significant threats to human security and societal progress (Adikari et al., 2009). The rapid increase in population, industrial production, and commercial activities, along with changes in water consumption patterns, has significantly elevated pollutant production in recent years, thereby deteriorating water quality (Alulema-Pullupaxi et al., 2021). UNESCO emphasizes that the declining quality of water is a growing threat to water security and sustainable development, creating a formidable challenge that affects both developed and developing countries globally (UNESCO, 2015).

Rivers in the United States, essential for various water needs, suffer from water quality degradation due to the influx of untreated sewage, industrial waste, oil spills, and other pollutants, with the discharge of untreated sewage and industrial effluents being a major factor contributing to elevated levels of harmful substances in water bodies (McLaughlin et al., 2020). According to the U.S. Environmental Protection Agency's (EPA) Toxics Release Inventory (TRI), industrial facilities in the United States discharged around 200 million pounds of hazardous materials into water bodies in 2021, including chemicals known to cause cancer, reproductive issues, and developmental problems (EPA, 2023). Major rivers such as the Mississippi, Ohio, and Missouri suffer significantly from these pollutants. For example, the Mississippi River, which flows through highly industrialized regions, is heavily impacted by the discharge of untreated sewage, industrial waste, and agricultural runoff, leading to elevated levels of hazardous substances like heavy metals and chemicals (McLaughlin et al., 2020). Similarly, the Ohio River has been identified as one of the most polluted rivers in the United States due to the significant amounts of toxic discharges from nearby industrial facilities (König et al., 2017). Furthermore, the Missouri River faces contamination from both industrial and agricultural sources, contributing to the degradation of water quality and posing risks to aquatic ecosystems and human health (Woodward et al., 2021). The natural purification processes for these contaminated waters are typically slow in water bodies (e.g., rivers); in cases of severe chemical pollution, the pollutants can persist and travel over long distances for several days before significant purification can occur (McGauhey, 1968; Peavy, 1986). This underscores the persistent and widespread effect that water pollution may have, supporting the need to identify where and to what extent mitigation strategies are required to protect human health and environmental integrity.

Flooding has the potential to disperse pollutants over extensive areas, affecting both residential zones and farmlands (Ponting et al., 2021). Specifically, the practice of constructing commercial, residential, and agricultural sites near rivers exacerbates this issue, as chemical pollutants from these activities can be mobilized by floodwaters and deposited onto downstream soils in the surrounding flood plains (Ponting et al., 2021). This situation increases health risks for communities who may come into direct or indirect contact with the contaminated areas and can cause significant damage to surrounding vegetation. Furthermore, chemically polluted floodwaters can infiltrate aquifers, compromising the quality of drinking water (Ponting et al., 2021).

Some communities are more susceptible to the effects of contaminant exposure due to age, pre-existing health conditions, or frequent exposure (Butter, 2006; Schwartz, 2007). Identifying hotspots where vulnerable communities are exposed to the risk of floodwaters with possible contamination has important implications for public health and resource allocation. For example, low-income communities, Indigenous populations, and other marginalized groups often suffer the most from river pollution's adverse effects in the United States, as they are disproportionately affected by the contamination of rivers (e.g., the Mississippi, Ohio, and Missouri) due to their proximity to industrial and agricultural pollution sources, which results in higher exposure to harmful substances (Hicks et al., 2021). Additionally, Indigenous communities rely heavily on river ecosystems for their cultural, spiritual, and subsistence needs, making them particularly vulnerable to the degradation of these water bodies (Allison & Cho, 2020). Studies suggest that these vulnerable communities experience higher exposure to harmful contaminants and consequent health issues than communities with fewer vulnerability indicators (Roder et al., 2017; Halder et al., 2015). One way to help mitigate the inequities in exposure is through the identification and mapping of these at-risk areas. Through this process, one can support targeted efforts to mitigate water contamination and further protect public health in communities with increased risk of exposure. Additionally, polluted rivers can have substantial economic impacts, including declining property values, decreased tourist numbers, and rising healthcare costs.

Assessing the risk of compound hazards involves quantifying vulnerability, the cost or amount of elements at risk, and the probability of occurrence (van Westen, 2004; Nelson et al., 2018). In the context of fluvial flood risk and contaminant transport, effective risk assessment

necessitates an understanding of the geographical location of communities in relation to pollutant sources, floodplains, and an overall measure of social vulnerability. Traditionally, risk assessment research and tools have focused on single risk factors, such as flooding or pollution, and evaluated these against the vulnerability of impacted communities (Tate et al., 2021; Nelson et al., 2015). For instance, conventional climate risk assessment models like HAZUS-MH are commonly used to estimate flood losses but do not account for contamination risks nor the vulnerability of communities in the impacted area (Scawthorn et al., 2006). The interconnected nature of waterways, pollutant sources, and community demographics requires a comprehensive approach that considers the interactions and cascading effects of various hazards, contamination issues, and social inequities.

Pinpointing areas where vulnerable communities are at risk from floodwaters with plausible contamination can help mitigate both health and economic impacts. This necessitates a thorough understanding of the prevalence of toxic chemical discharges, their relationship with flood zones, and the level of socio-economic vulnerability within the affected regions. In the southeastern United States, the Coosa River is a waterbody that has historically been impacted by non-point source pollution, with portions of the river highlighted as at risk by the Alabama Department of Environmental Management (ADEM, 2022). The 303(d) list, mandated by the Clean Water Act, is a catalog of impaired and threatened waters (streams, rivers, lakes, and coastal areas) that do not meet water quality standards. The significance of the 303(d) list lies in its role as a critical environmental management tool that identifies waterbodies failing to meet established water quality standards. Inclusion on the 303(d) list initiates the creation of Total Maximum Daily Loads (TMDLs), which are essential for restoring water quality by regulating pollutant levels. Portions of the Coosa River have been periodically listed on the 303d list which identifies those rivers and streams that show heightened levels of various pollutants. In addition, Gangrade et al. (2020) noted that probable maximum flooding estimate in the Alabama-Coosa-Tallapoosa (ACT) basin are most sensitive to the variables of meteorological forcing, climate change, antecedent soil moisture, reservoir storage, and land use land cover change. Future probable maximum flood events were estimated to be significant in the ACT. Thus, in the event of a flood in the Coosa River, there is a chance that contaminants will spread across the affected areas with the potential to disproportionately impact socially vulnerable communities.

The study aims to develop a spatial risk assessment framework using the Coosa River as a case study, to assess how social vulnerability and the likelihood of contamination associated with flood risk may change over time. Although the focus is on the Coosa River, the framework has been designed to be applicable to other riverine systems, providing a broader utility for assessing similar risks in different geographic contexts. This generalizability ensures that the findings and methodologies of this research can be adapted and applied to enhance environmental risk management and public health strategies across various regions facing similar challenges.

1.1 Research questions

This study encompasses two primary research questions, which are as follows:

1. What are the spatiotemporal patterns of Toxic Release Inventory (TRI) releases within the Coosa River watershed from 2000 to 2020?
2. How can a spatially explicit risk assessment framework be used to identify areas at risk of contamination due to flood exposure among socially vulnerable communities. What are the trends in these areas over the past two decades (2000-2020)?

1.2 Study area: Coosa River watershed

The Coosa River, traversing significant portions of Alabama and the northwestern quadrant of Georgia, has grappled with industrial discharge and non-point source pollution from agricultural activities, with the Alabama Department of Environmental Management (ADEM) documenting the detrimental impact of these residues on the river's health. This issue is exacerbated due to industrial operations discharge toxic chemicals into the environment, as evidenced by the 303(d) list for impaired waters (ADEM, 2024).

The Coosa River Basin Management Plan (1998) emphasizes the substantial risks posed by such contamination to human health and the broader ecosystem. Moreover, the Lower Coosa River Basin Management Plan (2005) identifies the region's susceptibility to flooding, which heightens the threat to nearby human settlements and properties. Historical records, such as those documented by Estis (2008), reveal numerous instances of severe rainfall and storm events leading to riverbank breaches and subsequent flooding of adjacent communities and Coosa River is no exception.

These flood events not only displace residents and damage homes but also exacerbate the spread of pollutants, creating compounded environmental and health hazards for those living near the river. The intersection of polluted waters and flood potential elevates the risk to communities, endangering both their health and safety. Figure 1.1 illustrates the location of the Coosa River watershed, defined by the Hydrologic Unit Code 8 (HUC 8) boundary, highlighting areas where communities face a higher probability of experiencing contamination due to flood events.

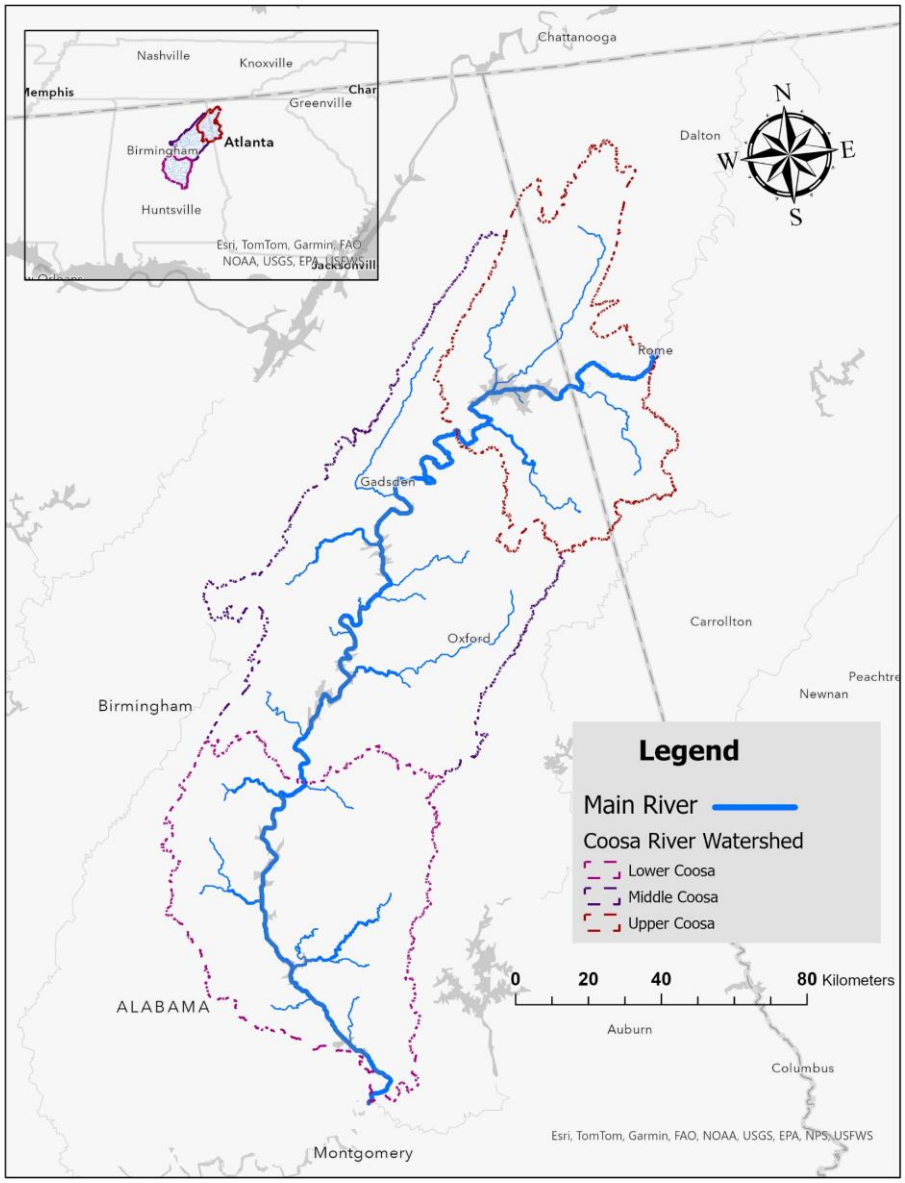

Figure 1.1: Location and HUC 8 delineated watershed boundary of the Coosa River watershed.

2. Review of literature

Flooding represents a significant concern both locally and globally, affecting an estimated 20 to 300 million people annually and accounting for approximately 40% of the world's natural disasters. This phenomenon poses serious challenges to societal stability and sustainable development worldwide (Euripidou and Murray, 2004; Hirabayashi and Kanae, 2009). Additionally, pollution in river systems has emerged as a major issue, often exacerbated during flood events when the discharge of pollutants from impaired rivers escalates considerably. The socio-economic and environmental impact of flooding is further intensified when one considered the potential for the dissemination of contaminants in flood waters, underscoring the urgency of addressing this complex and pervasive environmental issue (Crawford et al., 2021).

Previous studies provide substantial evidence linking industrial activities and their ancillary industries to the transport of pollution through river sediment (Ciszewski, 2001; da Rocha et al., 2017; Foulds et al., 2014; Guo et al., 2014; Lintern et al., 2016; Lynch et al., 2018; Rudis et al., 2009; Zak et al., 2009). These studies highlight the heightened risk of contaminants being dislodged and spread across catchment areas during flood incidents. For instance, Atoba et al. (2023) described how flood events in Galena Park, TX, redistributed toxic contaminants from industrial sites to residential areas, leading to potential waterborne diseases and chronic health conditions for individuals living in the neighboring areas. The severity of these impacts is influenced by the specific chemical concentrations in the region and the socio-economic factors that impact the frequency and duration of exposure.

Human activities such as industry, mining, and agriculture significantly increase the contamination risks for surrounding areas due to the pollutants they introduce. These pollutants can include heavy metals, radioactive substances, and acid mine drainage, which tend to accumulate within floodplains and sediment deposits (Abdel-Satar, 2017). Pollutants released from toxic facilities can enter fluvial systems through direct discharge and are subsequently transported by hydrological currents. As sediments move through these systems, they often settle in areas where water flow slows down, such as harbors, groin fields, lowland rivers, floodplains, wetlands, and estuaries, through sedimentation processes (Crawford et al., 2021). This sedimentation can later be disrupted by activities like dredging and erosion, leading to the re-release and distribution of contaminants into the environment. Large-scale flooding events

significantly exacerbate this process, causing widespread dispersal of pollutants into adjacent floodplains, ultimately impacting wildlife and human populations that rely on these environments through direct or indirect contact with the contaminated sediment or water (Crawford et al., 2021). For example, the 2012 floods in Kaziranga National Park in Assam, India, caused the death of hundreds of animals and led to widespread contamination from floodwaters carrying industrial chemicals and agricultural pesticides, impacting both the environment and wildlife (National Geographic Society, 2024).

For many flood prone areas, the heightened impact of a flood is primarily due to land use practices, increasing population growth in major urban centers and coastal areas, and the intensification of economic activities in flood-prone regions. As the frequency of flood events is expected to rise (Fadia et. al, 2019; Gao et. al, 2020), it becomes imperative to assess and mitigate the risks associated with potential societal, material, and financial damages (Rojas et al., 2013). Recent studies have shown that changes in land use and climate scenarios significantly affect future flood risks, underscoring the need for spatial and temporal analysis (Lin et al., 2020; Rezende et al., 2019). For example, the Pearl River Delta in China is expected to see increased flood risks due to urban expansion and climate change, highlighting the importance of integrating these factors into flood risk management strategies (Zhu et al., 2024).

Additionally, recent storm activities have highlighted the negative impacts of flooding on the environment and infrastructure, particularly in urban areas and around wastewater facilities that contribute to the dispersion of pollutants during flood events. For example, case studies of coastal flooding caused by tropical storms like Hurricane Katrina in 2005 and Hurricane Harvey in 2017 in the United States, demonstrated a marked increase in exposure to carcinogenic compounds among low-income communities. For both these cases, flooding facilitated the widespread redistribution of these harmful substances to areas where communities commonly congregated (outside homes, parks, and streets) (Horney et al., 2018). Furthermore, research by Bodenreider et al. (2019) indicated that floodwaters during Hurricane Harvey disproportionately transported contaminants to low-income communities of color. Important to keep in mind is that extreme weather events, which are among the costliest natural disasters in terms of infrastructure and economic damage, also significantly influence the dispersal and concentration of pollutants.

This dispersal can lead to both immediate and long-term exposure to contaminants for affected communities (Chagué-Goff et al., 2012; Goto et al., 2012; Horney et al., 2018; Iqbal et al., 2007).

Vulnerability, defined as the ability of an individual or group to predict, manage, withstand, and recover from natural hazards, is influenced by a variety of social, economic, and political factors that dictate how severely these hazards impact different populations (Blaikie et al., 1994). Research consistently highlights that historically underrepresented groups are particularly vulnerable to natural hazards, primarily because they are more likely to live in flood-prone areas that are also close to toxic release facilities. This proximity to multiple hazards can significantly amplify the adverse impacts and health outcomes experienced by these populations (Collins et al., 2018; Shrader-Frechette & Biondo, 2021; Maantay & Maroko, 2009). For example, Atoba et al. (2023) detailed how hazardous pollutants from industrial areas were transferred to residential neighborhoods in Galena Park, TX, during flooding events, with particularly severe health implications for socially vulnerable groups in the area. Those residing in the housing near hazard-prone zones not only face increased exposure to these dangers but also lacked the robust social, financial, or political support needed to mitigate and recover from such events, leading to greater losses and extended recovery periods compared to their more affluent or socially secured counterparts (Mitchell, 1999).

Evaluating the overall risks and vulnerabilities of different communities to hazards can be effectively achieved through a comprehensive risk analysis framework. Such frameworks facilitate systematic evaluations of the risks associated with multiple hazards and their impact on vulnerable communities, such as those posed by contaminated floodwaters. One approach is to holistically combine multiple risk indicators and criteria to understand the key factors (geographic and analytic) contributing to hazard exposure (Abdrabo et al., 2023). Developing an effective framework requires interdisciplinary collaboration and the integration of diverse sources of information representing the hazards and communities in the impacted areas (de Moel et al., 2015). The initial step in this process involves assessing the compound flood hazard by focusing on the likelihood and severity of potential flood events and the associated distribution and discharge levels of toxic release points (Pappenberger et al., 2012; Alfieri et al., 2013). By overlaying this hazard data with socio-economic data (Jongman et al., 2012) and combining it to generate a vulnerability index (de Moel et al., 2015), researchers can identify areas where the

most vulnerable communities are most likely to be exposed to floodwaters with plausible contamination. This integrated approach allows for a deeper understanding of high-risk zones, enabling targeted interventions and resource allocations to mitigate the risks and protect vulnerable populations effectively.

The Coosa River has experienced severe water quality degradation due to a history of discharge from industrial and agricultural activities. Much of this discharge and the associated water impairment is documented in ADEM's 303(d) list of impaired waterbodies with portions of the in Cherokee, DeKalb, Etowah, St. Clair, and Talladega counties appearing semi-regularly. The Coosa River is also recognized by some organizations as one of the most polluted rivers in the United States, primarily due to the impact of industrial and agricultural pollution (American Rivers, 2022). That said, a thorough investigation of where discharge from TRI facilities is introduced into the waterway is largely absent from the literature. This makes it difficult to identify the portions of the waterway where chemicals and heavy metals may interact with the river system. As a result, the Coosa watershed serves as a prime study area to demonstrate the effectiveness of the proposed methodological framework.

This study aims to highlight the ability of the proposed methodological framework to combine multiple sources of data related to compound hazards. It does so by identifying the areas in the Coosa watershed where discharge from industrial activities will be concentrated, and how that interacts with flood prone areas and socially vulnerable communities. While numerous studies have documented the adverse health outcomes and environmental degradation caused by water pollution (Majeed & Ozturk, 2020; Siddiqua et al., 2022; Lin et al., 2022; Sonone et al., 2020), there remains a gap in the research related to how areas experiencing compound hazards are identified, specifically at the intersection of flooding and chemical discharge. Furthermore, there is a need to address the vulnerability of communities in these areas, which are often less equipped to cope with the resultant health and environmental disparities. To address this research gap, this study develops a framework capable of integrating the location of agricultural and industrial activity, flood prone areas, and community vulnerability. This framework is applied to the Coosa River watershed to understand the temporal and spatial changes in how TRI discharge, vulnerability, and flood exposure have varied over time.

3. Methods:

Identifying the spatial and temporal distribution of Toxic Release Inventory (TRI) facilities within the Coosa River watershed is crucial for understanding both the geographic dispersion and temporal trends of toxic chemical releases. This approach illustrates how TRI facilities are distributed over time and the quantities of toxic chemicals released into the water. Additionally, it provides insight into whether certain locations consistently experience high levels of toxic emissions over time. This analysis involves the application of advanced geospatial techniques, including the space-time cube and emerging hotspot analysis. The space-time cube method allows for the visualization and analysis of data across both spatial and temporal dimensions, thereby identifying patterns and trends that may not be noticeable through traditional methods. Emerging hotspot analysis further enhances this by detecting areas that have changes in the intensity of toxic releases, pinpointing regions that are becoming increasingly problematic.

The compound hazard framework is a data-driven approach that uses a detailed weighting scheme to evaluate the impact of various risk factors, such as socio-economic vulnerability, pollution hazards, and flood hazards on the overall risk score. This method involves crucial steps, starting with the collection and preparation of diverse datasets, ensuring that the analysis is based on accurate and reliable information. By integrating these different data sources, the framework can identify regions at higher risk where vulnerable communities may face challenges due to contamination potentially dispersed by flooding. This comprehensive approach not only provides a thorough understanding of the risks but also supports more informed decision-making and efficient resource allocation. The ability to merge various datasets into a single assessment tool highlights the framework's robustness, making it essential for evaluating complex risk scenarios and contributing to more effective and sustainable hazard management practices.

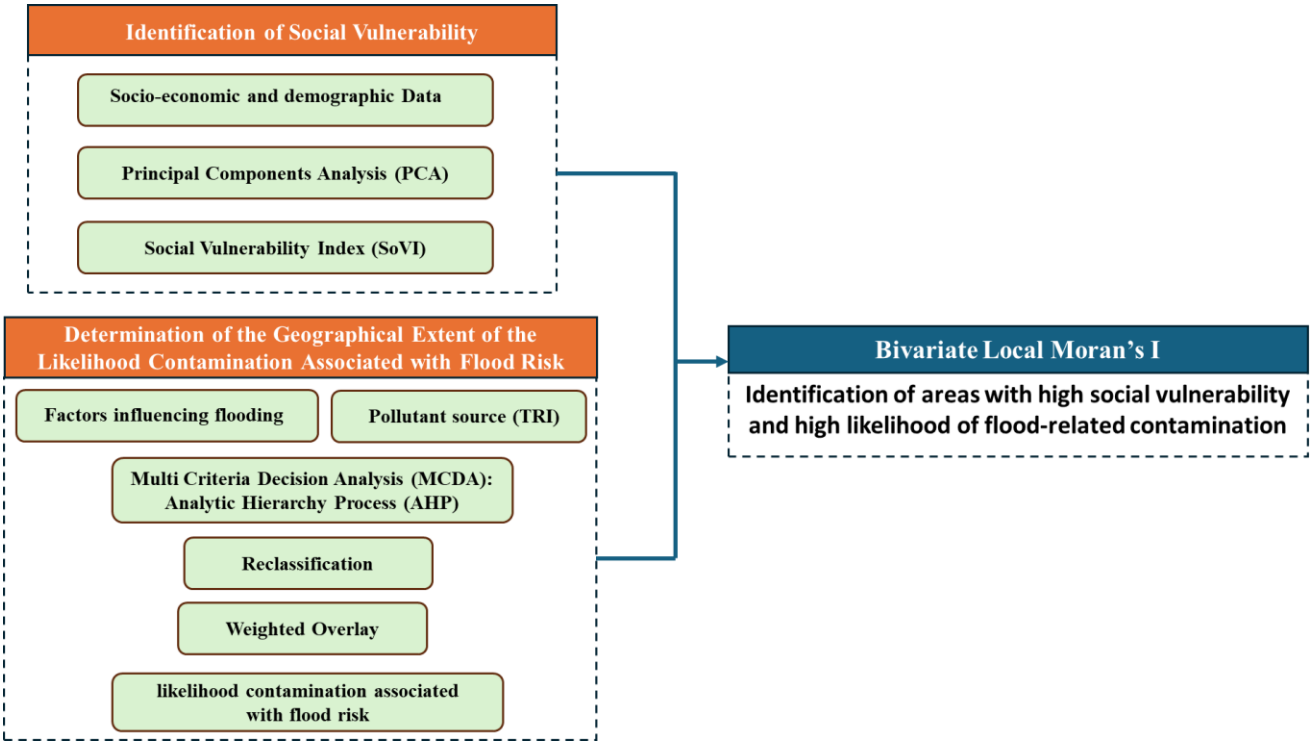

Figure 3.1: Methodological diagram illustrating the analysis steps for the compound hazard framework.

3.1 Data background

3.1.1 Toxic Release Inventory (TRI) data

For this study, the Toxic Release Inventory (TRI) data will be utilized as the pollutant source (US EPA, 2023). A facility qualifies as a TRI if it manufactures, processes, or otherwise uses significant quantities of toxic chemicals specified by the Environmental Protection Agency (EPA) and meets certain threshold levels of chemical usage and employee numbers. These facilities are required to report their annual chemical releases to the EPA under the Toxic Release Inventory (TRI) program, which has published pollutant discharge data annually since the establishment of the Emergency Planning and Community Right-to-Know Act (EPCRA) in 1986. It aims to provide the public with crucial information about the release of toxic chemicals by industrial and federal facilities.

The TRI dataset includes detailed information on the location of each TRI facility, the total amount of pollutants discharged, the types of pollutants, and the discharge mediums (air, water, land). For this study, the total amount of chemicals used or released by the facilities that fall within the boundary of the Coosa River watershed is considered. Through a comprehensive

analysis of the TRI dataset, the changing locations and densities of toxic releases over two decades (2000 to 2020) have been identified. This analysis facilitates the observation of how these variations have influenced the contaminated flooding scenarios in the years 2000, 2010, and 2020. The TRI data has been integrated as a pollution source with other flood indicators to assess the patterns of toxic releases and their influence on flood contamination over the years.

3.1.2 Socio-economic and demographic data

To determine the level of community vulnerability to compound hazards, data describing the socio-economic conditions of the communities have been utilized. This data has been sourced from the National Historical Geographic Information System (NHGIS) of the Integrated Public Use Microdata Series (IPUMS) and gathered at the United States (US) Census block group level for three different years (2000, 2010 and 2020). The NHGIS is a project funded by the National Science Foundation (NSF) with a primary objective of compiling US census data at various aggregation levels and years which encompass both geographical and attribute data (McMaster & Noble, 2005; Schroeder & McMaster, 2007). The specific socioeconomic variables used in this study are detailed in Table 3.1.

Table 3.1: List of data, description, and source for social vulnerability.

Data	Description	Source
Total Minority	Number of Black or African American, American Indigenous, Asian, Native Hawaiian, Hispanic, and Other	National Historical Geographic Information System (NHGIS) database from Integrated Public Use Microdata Series (IPUMS) (https://www.nhgis.org/)
Education less than high school	Number of people who have attained not more than high school	
Income less than poverty line	Number of people who have income less than poverty line	
Median household income*	Median household income of the block group (Reversed)	

Per capita income*	Per capita income of the block group (Reversed)	
Median gross income*	Median gross income of the block group (Reversed)	
Child population	Number of population <18 years of age	
Aged population	Number of population ≥ 65 years of age	
House owner	Number of house owners	
House renter	Number of house renters	
Mobility	Housing units with no car	

The measurement of community social vulnerability requires the use of multiple socio-economic indicators that have been observed as influential when it comes to the initial impact of an event and the rate of community recovery (Fekete, 2009). 'Total Minority' captures the proportion of minority populations, as these groups often face greater challenges and disparities during hazardous events. 'Education less than high school' is a variable reflecting the educational attainment of the population, indicating that lower educational levels can limit access to crucial resources and information for disaster preparedness and recovery. The variable 'Income less than poverty line' highlights the economic vulnerability of households living below the poverty threshold, who typically have fewer financial resources to cope with and recover from hazards.

'Median household income' and 'Per capita income' are two variables that are important to assess overall economic well-being of the community, with higher income levels generally correlating with greater capacity for mitigation and recovery. The variable 'Median gross income' provides additional insight into the financial stability of households, further informing the economic dimension of vulnerability. The 'Child population' variable is crucial as children are more susceptible to disaster impacts, requiring special consideration.

'Aged population' is a variable which accounts for the elderly, who may have limited mobility and increased sensitivity to contaminant exposure that heighten their vulnerability during emergencies. 'House owner' and 'House renter' variables differentiate between homeowners and

renters, recognizing that renters may have fewer resources and less stability, increasing their vulnerability. Finally, the 'Mobility' variable gauges the population's ability to evacuate or relocate (people having cars/vehicles), with lower mobility potentially exacerbating the impacts of hazardous events. These variables collectively provide a comprehensive assessment of social vulnerability, aiding in identifying at-risk populations and allocating resources for mitigation and response efforts. Utilizing this dataset, the analysis seeks to offer a detailed understanding of community vulnerability, categorizing it into five distinct levels: low, moderately low, medium, moderately high, and high social vulnerability.

3.1.3 Flood risk data of the polluted river

In this study, eleven parameters have been employed to generate contaminated flood water hazard maps for the study area. Data for these parameters were collected for the same three years as the socio-economic indicators (2000, 2010, and 2020) to capture changes in flood risk over time. These parameters include Digital Elevation Model (DEM), slope, precipitation, distance from the main river, distance from Toxic Release Inventory (TRI) sites, Topographic Wetness Index (TWI), Land Use/Land Cover (LULC) map, drainage density, and TRI density (Parsian et al., 2021). These parameters are detailed in Table 3.2.

Table 3.2: List of data and source for contaminated flood risk

Flood Potential	
Data	**Source**
Digital Elevation Model (DEM)	United States Geological Survey (USGS) (https://www.usgs.gov/)
Slope	Generated from DEM in ArcGIS Pro
Flow Accumulation	Generated from DEM in ArcGIS Pro
Precipitation	PRISM High-Resolution Spatial Climate Data (https://prism.oregonstate.edu/)
Land Use/Land Cover (LULC)	National Land Cover Database (https://www.usgs.gov/centers/eros/science/national-land-cover-database)
Distance from the main river	Generated from DEM in ArcGIS Pro
Topographic Wetness Index (TWI)	Generated from DEM in ArcGIS Pro
Normalized Difference Vegetation Index (NDVI)	Google Earth Engine (Landsat 8) (https://earthengine.google.com/)
Drainage density	Generated from DEM in ArcGIS Pro

Pollution Potential	
Data	**Source**
Distance from TRI	US Environmental Protection Agency (EPA) (https://www.epa.gov/)
TRI density	US Environmental Protection Agency (EPA) (https://www.epa.gov/)

To develop a contaminated flood risk map, the 'Digital Elevation Model (DEM)' with 30-meter spatial resolution is utilized to provide detailed information on the terrain, essential for understanding water flow and floodplain delineation. 'Slope' is included as it influences the speed and direction of surface runoff, impacting flood risk and the potential spread of contaminants. 'Flow Accumulation' helps identify areas where water converges, indicating zones of higher flood potential and potential contaminant concentration. Slope can be calculated from the DEM using the 'Slope' tool, and Flow Accumulation can be calculated using the 'Flow Accumulation' tool, both found in the Spatial Analyst toolbox in ArcGIS Pro.

'Precipitation' data is critical as it directly impacts the volume of water contributing to floods, influencing both the extent and intensity of flooding events. For this study, annual average precipitation data has been sourced from the PRISM High-Resolution Spatial Climate Data, which originally had an approximate spatial resolution of 4 kilometers. To ensure consistency with other parameters in our dataset, this data was resampled to a 30-meter spatial resolution using the 'Resample' tool in ArcGIS. This resampling process is vital as it allows for more detailed and accurate analysis, enabling better integration and comparison with high-resolution datasets (10 other parameters) used in our study. The precision in resampling ensures that our data maintains its integrity while becoming more suitable for localized (block groups wise) flood modeling and risk assessment. Resampling methods, such as nearest-neighbour resampling and regression-based downscaling, have been proven effective in preserving spatial correlations and improving the resolution of precipitation data (Wojcik & Buishand, 2003; Wilby et al., 2003).

'Land Use/Land Cover (LULC)' information is used to understand how different land surfaces interact with water flow, with urban and industrial areas potentially contributing to higher contamination levels. The 'Distance from the main river' is a key variable, as proximity to rivers increases the likelihood of flooding and the subsequent spread of contaminants. The distance from the main river streams is computed using the 'Euclidean Distance' tool in ArcGIS Pro with 30-meter spatial resolution.

The ‘Topographic Wetness Index (TWI)’ characterizes the water accumulation trend at a specific location, while the local slope elucidates the influence of gravitational forces on water flow (Fernandez & Lutz, 2010). TWI is extensively utilized to predict soil moisture levels and delineates the propensity of an area to accumulate water (Beven & Kirkby, 1979). In this study, the slope and DEM data was employed to calculate TWI using the following equation 1:

$$\text{TWI} = \ln (AS / \tan \beta) \quad (1)$$

Where, AS represents the specific catchment area, and β is the local slope angle in degrees.

The ‘Normalized Difference Vegetation Index (NDVI)’ provides insights into vegetation health and density, which can affect water absorption and runoff patterns. For this study, the NDVI data was obtained from Google Earth Engine, utilizing Landsat 8 imagery, and was processed to a spatial resolution of 30 meters for the study area.

The ‘Distance from TRI’ gauges the distance from the toxic chemical release sites which is included to measure proximity to potential contaminant sources, essential for assessing the risk of hazardous substance dispersion during floods. This distance was calculated for all locations relative to existing TRI facilities using the Euclidean Distance tool in ArcGIS Pro, providing essential data for comprehensive risk assessment.

‘TRI density’ quantifies the concentration of TRI sites based on the total toxin release to surface water within a specified area, highlighting regions with a heightened likelihood of contamination. Utilizing the ‘Kernel Density’ tool in ArcGIS Pro, this density was calculated with the value field representing the amount of toxic chemical release, thereby delineating areas of higher toxic release density within the study area.

Lastly, ‘Drainage density’ is used to understand the efficiency of water removal from the landscape, influencing flood dynamics and potential contaminant spread. Drainage density was calculated using the following equation 2:

$$DD = \frac{\sum_1^n \mathrm{L}}{F} \quad (2)$$

Where L represents Length of the streams, N is the number of streams, and F is the contributing drainage area. Higher drainage density values indicate lower infiltration rates and higher surface flow velocity (Dragičević, et. al, 2019).

In this study, the data for the Digital Elevation Model (DEM) and other parameters dependent on DEM, including flow accumulation, distance from the main river, slope, Topographic Wetness Index (TWI), and drainage density, were collected only for the year 2020.

This decision was based on the availability and quality of the 2020 data, which represents the most accurate and comprehensive dataset for these parameters. Studies have shown that DEM-related parameters do not undergo significant changes over short periods, making it reasonable to use the 2020 data consistently across all three scenarios (2000, 2010, and 2020) (USGS, 2020; Li et al., 2021; Jones et al., 2018)). Therefore, to ensure consistency and reliability the 2020 data for these parameters were used in the analysis.

For the remaining parameters, such as precipitation, land use/land cover (LULC), normalized difference vegetation index (NDVI), distance from TRI, and TRI density, data were collected for the years 2000, 2010, and 2020. These parameters were chosen for each specific year because they exhibit changes over time and play a crucial role in the assessment of contaminated flood risk. These variables collectively provide a comprehensive assessment of contaminated flood risk, enabling the identification of high-risk areas and informing mitigation strategies.

The compound hazard framework operates under assumption that reflect the current understanding of how flooding and contaminant transport likely interact in the environment. It is assumed that areas in close proximity to sources emitting large quantities of toxic substances are at a heightened risk of contaminant exposure during flood events compared to more distant locations (Conley, 2011).

3.2 Data analysis

3.2.1 Spatial-temporal analysis

This study used the Space Time Cube analysis in ArcGIS Pro to explore the trends in Toxic Release Inventory (TRI) densities in terms of total releases in water in the Coosa River watershed from 2000 to 2020, analyzing data every two years. This method allowed to combine spatial and temporal data into specific geographic locations, to observe how pollution patterns changed over time. Each section of the cube represents a specific time period and location, with trends calculated using the Mann-Kendall test. This test looks at how values change over time, helping us understand the broader patterns of TRI water releases (ESRI, 2021a; Kendall & Gibbons, 1990; Mann, 1945). The Mann-Kendall test works by comparing pairs of time points, assigning a score of 1 if the value increased, -1 if it decreased, and 0 if there was no change. The overall trend is found by summing these scores, with a total of zero indicating no clear trend. The significance of this trend is then determined using statistical measures, including a z-score and p-value. A low p-

value means the trend is significant, while the sign of the z-score shows whether the trend is upward or downward (ESRI, 2021a).

The test statistic S is calculated using the following formula:

$$S = \sum_{i=1}^{n-1} \sum_{j=i+1}^{n} a_{ij} \tag{3}$$

where,

$$a_{ij} = sign(x_j - x_i) = sign(R_j - R_i) = \begin{cases} 1 & x_i < x_j \\ 0 & x_i = x_j \\ -1 & x_i > x_j \end{cases} \tag{4}$$

The ranks of x_i and x_j time series are defined as R_i and R_j, respectively. Assuming the data are independent and identically distributed, the mean and variance of *S* statistics are,

$$E(s) = 0 \tag{5}$$

$$V_o(S) = \frac{n(n-1)(2n+5)}{18} \tag{6}$$

Where n is the number of observations. This results in a reduction of the variance of *S* due to the existence of tied ranks (equal observations).

$$V_o^*(S) = \frac{n(n-1)(2n+5)}{18} - \sum_{j=1}^{m} \frac{t_j(t_j-1)(2t_j+5)}{18} \tag{7}$$

Where m is the number of groups of tied ranks, each with t_j tied observation. The methods iterate over the independent data and calculate the exact distribution of *S*. The method makes the *S* closer to a normal distribution with the observation increment, which means the more the study time, the more accurate the model.

3.2.2 Emerging hotspot analysis

The Space Time Cube has been utilized to identify temporal trends in TRI density in terms of total release to water by detecting spatial hotspots that emerge or persist over time (ESRI, 2021; Getis & Ord, 1992; Ord & Getis, 1995). This approach employs Getis-Ord local statistics to analyze the reduction of variance from equation 7, using the following equation 8 to calculate the z-score:

$$G_i^* = \frac{\sum_{j=1}^{n} w_{i,j}x_j - \bar{X}\sum_{j=1}^{n} w_{i,j}}{S\sqrt{\frac{\left[n\sum_{j=1}^{n} w_{i,j}^2 - \left(\sum_{j=1}^{n} w_{i,j}\right)^2\right]}{n-1}}} \quad (8)$$

Where x_j is the attribute value for feature j, $w_{i,j}$ is the spatial weight between feature i and j, *and* n is the total number of features. The calculation of $\bar{X}$ and S is followed by Equations 9 and 10.

$$\bar{X} = \frac{\sum_{j=1}^{n} x_j}{n} \quad (9)$$

$$S = \sqrt{\frac{\sum_{j=1}^{n} x_j^2}{n} - (\bar{X})^2} \quad (10)$$

Using the Mann-Kendall test statistics, the analysis identified sixteen distinct spatial-temporal clusters (ESRI, 2021). These clusters were classified into various categories based on their significance and temporal characteristics. A "New Hot Spot" emerges as a statistically significant hot spot for the first time in the most recent observation period. A "Consecutive Hot Spot" is significant for at least two sequential time steps towards the end of the observation period, with less than 90% overall significance. An "Intensifying Hot Spot" shows significant clustering in more than 90% of the time steps, with increasing intensity. A "Persistent Hot Spot" remains significant across more than 90% of the time steps without a trend in clustering intensity, while a "Diminishing Hot Spot" shows a significant decline in clustering intensity over more than 90% of the periods. A "Sporadic Hot Spot" appears irregularly, being significant only in the last time step, and an "Oscillating Hot Spot" alternates between hot and cold statuses, being significant in less than 90% of intervals. A "Historical Hot Spot" was significant in at least 90% of earlier intervals but has lost current significance. Similarly, cold spots are categorized as "New," "Consecutive," "Intensifying," "Persistent," "Diminishing," "Sporadic," "Oscillating," and "Historical Cold Spots," reflecting areas of low counts or clustering with analogous criteria to hot spots. This detailed categorization reveals the complex patterns of spatial-temporal variation, underscoring their importance in geography and environmental studies.

3.2.3 Social Vulnerability Index (SoVI)

Cutter et al. (2003) developed the Social Vulnerability Index (SoVI) to identify communities that are particularly susceptible to harm based on a combination of variables related to socioeconomic status, demographic groups, housing and mobility (Table 3.1). The creation of this index can take many forms but is most commonly created using the Principal Component

Analysis (PCA) approach. This approach transforms the raw data into distinct components that represent different aspects of social vulnerability. For example, we might expect to see high poverty rates and low educational attainment correlate together as they both indicate economic and social disadvantages, contributing to higher overall vulnerability. Similarly, high renter occupancy and low homeownership rates may also cluster together, reflecting housing instability and reduced capacity to recover from disasters. By using PCA, these correlated data are converted into a smaller subset of components which serve as the optimal linear representation of the dataset's multivariate point cloud. The resulting components simplify the original set of variables by combining those that are similarly correlated while maximizing the variance that each component represents in the dataset.

To calculate and capture changes in SoVI over time and to assess how that interacts with flooding and pollution, three separate PCAs were performed using the same set of 11 variables (Table 3.1) for the years 2000, 2010, and 2020. All PCA analyses were conducted using the analytical software GeoDA. GeoDA is a spatial and data analysis software package that includes options for conducting Principal Component Analysis (PCA) (Anselin et. al, 2022) among other things. Within GeoDA, there are two distinct PCA methods available: Singular Value Decomposition (SVD) and Eigen. Both methods can utilize three types of data transformations: Standardize (Z), Standardize (MAD), and Range Standardize. These transformations differ in their approaches to standardizing data, and it is recommended to evaluate all three when conducting a PCA to determine the most suitable method for the analysis (Anselin et. al, 2022).

Table 3.3 presents the PCA results for all the methods. Among the various combinations, the Singular Value Decomposition (SVD) with Range Standardization captures the highest variance in the first principal component (PC1). To develop the final Social Vulnerability Index (SoVI) for the years 2000, 2010, and 2020, the first four principal components (PC1, PC2, PC3, and PC4) were summed together. This approach is justified by the high proportion of variance explained by these four principal components. Specifically, the sum of the variances for the first four principal components (PC1, PC2, PC3, and PC4) using the SVD-Range Standardize method accounts for 0.93, 0.98, and 0. 98 of the total variances for the years 2000, 2010, and 2020, respectively (Table 3.3).

Table 3.3: Principal Component Analysis (PCA) results (for 2000, 2010 and 2020)

Year	Combination	PC1	PC2	PC3	PC4	Total
2000	SVD-Z	0.34	0.26	0.12	0.08	0.82
	SVD-MAD	0.36	0.25	0.13	0.08	0.83
	SVD-Standardize	**0.74**	0.11	0.04	0.02	**0.93***
	Eigen-Z	0.34	0.26	0.12	0.08	0.82
	Eigen-MAD	0.34	0.26	0.12	0.08	0.82
	Eigen-Standardize	0.72	0.09	0.05	0.04	0.92
2010	SVD-Z	0.34	0.26	0.12	0.08	0.82
	SVD-MAD	0.36	0.25	0.13	0.08	0.83
	SVD-Standardize	**0.91**	0.03	0.01	0.01	**0.98***
	Eigen-Z	0.30	0.26	0.12	0.08	0.77
	Eigen-MAD	0.30	0.26	0.12	0.08	0.77
	Eigen-Standardize	0.78	0.06	0.05	0.03	0.93
2020	SVD-Z	0.28	0.20	0.12	0.10	0.72
	SVD-MAD	0.29	0.18	0.13	0.10	0.72
	SVD-Standardize	**0.93**	0.02	0.01	0.01	**0.98***
	Eigen-Z	0.28	0.20	0.12	0.10	0.72
	Eigen-MAD	0.28	0.20	0.12	0.10	0.72
	Eigen-Standardize	0.70	0.10	0.04	0.04	0.89

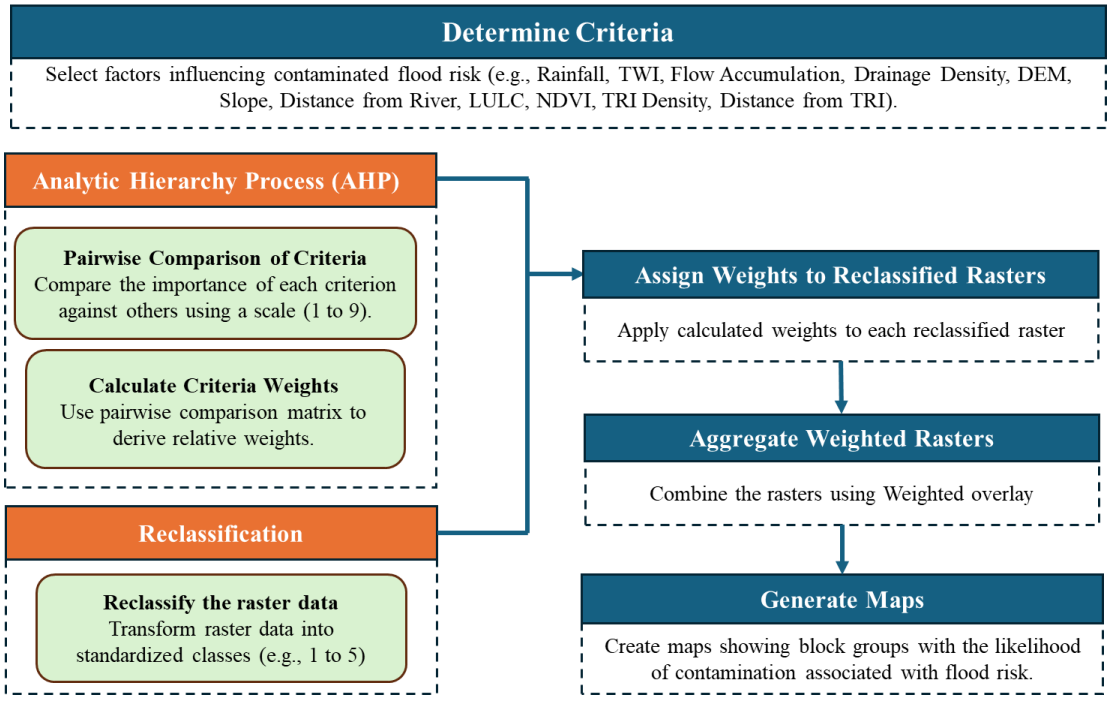

Figure 3.2: Methodological diagram for generating maps showing the likelihood of contamination associated with flood risk for the years 2000, 2010 and 2020.

3.2.4 Utilization of Multi-Criteria Decision Analysis (MCDA)

In this case study of the Coosa River watershed, Multi-Criteria Decision Analysis (MCDA) techniques have been applied to determine the importance of geographical parameters and emission sources (TRIs) associated with the compound hazard. MCDA is an analytic technique that takes as input multiple pieces of information and combines them in a manner that allows one to identify where and to what extent these parameters correspond across a given spatial extent (Hermans et al., 2007; Greene et al., 2011). As previously mentioned, one of the primary objectives of this study is to identify contamination risk areas during or following flood events due to the potential mixing of chemicals emitted from TRI facilities with floodwater. This approach aligns with the understanding that compound flood events are driven primarily by excessive water, the area's topographical characteristics, and the locations of chemical-emitting industries that discharge into surface water. The Analytical Hierarchy Process (AHP) is one MCDA technique that is suitable for regional studies (Souissi et al., 2019). Like other MCDA techniques, one of the most important steps in AHP is determining the importance that each variable under consideration has on the final output. AHP provides an analytic approach for ranking variables by importance using a unique weighting scheme. Moreover, AHP is recognized as a straightforward, and optimal method for integrating multiple factors in decision-making processes to create flood hazard maps with a high degree of accuracy (Danumah et al., 2016). For the AHP approach, weight of the parameters is allowed to vary depending on the purpose of the research and landscape characteristics and it is important to recognize that different studies have weighed parameters differently to match their study contexts. For instance, Mahmoud and Gan (2018) identified runoff and flow accumulation as dominant factors, while Kazakis et al. (2015) and Souissi et al. (2019) emphasized the significant impact of elevation. Other studies, such as Vojtek and Vojteková (2019), highlighted slope and river density as critical factors, and Al-Abadi (2016) pointed to the stream power index (SPI) as a central determinant. Nevertheless, this technique may introduce elements of ambiguity and bias, as it relies on the expertise, opinions, and knowledge of experts (Pourghasemi et al., 2014).

3.2.5 Analytic Hierarchy Process (AHP)

The Analytic Hierarchy Process (AHP) is a structured technique for decision-making and has been applied in several environmental risk assessment contexts (Parsian et al., 2021). It involves structuring multiple criteria into a hierarchical format by assessing their relative importance, comparing solutions for each criterion, and ultimately ranking the alternatives based on factors like cost, benefit, or risk (Saaty, 1997; Saaty, 1980).

AHP is leveraged here to determine the weights (importance) of the input factors for building a contaminated flood water hazard map. The weight values for each criteria are ascertained using a pairwise comparison matrix, developed with insights from relevant literatures and local experts (Sepehri et. al, 2020). This matrix is normalized by dividing each element by the sum of its column and the average of each row will serve as the final weight for the respective parameter (Saaty, 1980).

Table 3.4: Importance scale in analytical hierarchy process (AHP) (for 2000, 2010 and 2020)

Numerical value	Description
1	Equal importance to element 1 and 2
3	Moderate importance of element 1 over element 2
5	Strong importance of element 1 over element 2
7	Very strong importance of element 1 over element 2
9	The extreme importance of element 1 over element 2
2,4,6,8	Intermediate values

In this study, the relative importance of the selected factors is ranked on a scale from 1 (least importance) to 9 (highest importance) (Table 3.4) where importance is determined by that variables contribution to the overall compound hazard risk. Each pair of variables is compared to one another and assigned a numerical value from the importance scale to indicate their relative significance. These are the values that are used to calculate weights. Linear normalization of the matrix for pairwise comparison is performed by summing the values of each column and then dividing each component of the matrix by its respective total (Table 3.5).

To validate the accuracy and appropriateness of weight determination in AHP, the Consistency Ratio (CR) is employed to measure the consistency among the weight values of various parameters (Equation 11). A CR value of 0.1 or below indicates an acceptable level of consistency in the pairwise comparison matrix. This ensures that the comparisons between all variables remain consistent within the matrix. For example, if variable A is deemed more important than variable B, and variable B is more important than variable C, then variable A should logically be more important than variable C. Inconsistent comparisons (e.g., if A is less important than C somewhere is the matrix) would lead to a higher CR value, indicating a need for re-evaluation of the pairwise comparisons. In contrast, values exceeding 0.1 suggest the matrix needs reevaluation because high CR values indicate inconsistencies in the judgments made during the pairwise comparisons. The computation of CR involves determining λ_{max} (the highest eigenvector) and the Consistency Index (CI), as outlined in Equations (12) and (13), respectively.

$$CR = \frac{CI}{RI} \tag{11}$$

$$\lambda_{max} = \frac{1}{n}\sum_{i=1}^{n} \frac{a_{ij \times w_i}}{w_i} \tag{12}$$

$$CI = \frac{\lambda_{max} - n}{n - 1} \tag{13}$$

where RI is the Random Index, a value that represents the average consistency index of a large number of randomly generated matrices of the same order (Golden & Wang, 1989), a_{ij} is pairwise comparison matrix element, and w_i is the weight value of each parameter.

The weights were determined by calculating the average of the normalized matrix values for each row (Table 3.6). The CR of the generated weights is 0.06, which is below the threshold of 0.1, indicating that the evaluations are sufficiently consistent and validating the procedure for detecting the impact of each criterion on flooding.

The weights are then determined by calculating the average of the normalized matrix values for each row (Table 3.6). The CR of the generated weights is 0.06, which is below the threshold of 0.1, indicating that the evaluations are sufficiently consistent and validating the procedure for detecting the impact of each criterion on flooding. These weights have been used in the resulting

overlay process (detailed below) to generate the compound flood hazard zones. Table 3.7 presents the resulting weight values.

Table 3.7 shows that, with a weight value of 0.1436 (14%), precipitation has been identified as the criterion with the highest importance for identifying flood prone areas. The weights for flow accumulation and slope, with values of 0.1375 and 0.1268 (14% and 13%), respectively, also indicate a high potential for flooding. DEM and distance to river have been assigned weights of 0.1183 and 0.0912 (12% and 9%), respectively, underscoring their importance in determining the potential for flood risk in this area. Next, TRI density and distance from TRI have weights of 0.0892 and 0.0651 (9% and 7%), respectively, highlighting their role in assessing contamination risks. Other criteria such as drainage density, TWI, LULC, and NDVI have been weighted based on their contribution or influence on contaminated flood risk as determined by the AHP analysis. These weights have been applied to create all the contaminated flood scenarios for the years 2000, 2010, and 2020.

Table 3.5: Pairwise comparison matrix for the eleven parameters by analytical hierarchy process (AHP) (for 2000, 2010 and 2020).

Factors	Precipitation	Slope	Flow Accumulation	DEM	Distance to River	Drainage Density	TWI	LULC	Distance from TRI	TRI density	NDVI
Precipitation	1	2	2	1	2	2	3	2	2	1	3
Slope	1/2	1	1	3	2	3	3	1	1	1	3
Flow Accumulation	1/2	1	1	2	2	3	3	2	3	1	4
DEM	1	1/3	1/2	1	3	2	3	2	2	1	4
Distance to River	1/2	1/2	1/2	1/3	1	2	3	3	1	1	3
Drainage density	1/2	1/3	1/3	1/2	1/2	1	2	2	2	1	4
TWI	1/3	1/3	1/3	1/3	1/3	1/2	1	1	2	1	3
LULC	1/2	1	1/2	1/2	1/3	1/2	1	1	1	1	3
Distance from TRI	1/2	1	1/3	1/2	1	1/2	1/2	1	1	1	3
TRI density	1	1	1	1	1	1	1	1	1	1	3
NDVI	1/3	1/3	1/4	1/4	1/3	1/4	1/3	1/3	1/3	1/3	1
Sum	6.67	8.83	7.75	10.42	13.50	15.75	20.83	16.33	16.33	10.33	34.00

Table 3.6: Normalized pairwise comparison matrix for the eleven parameters by analytical hierarchy process (AHP) (for 2000, 2010 and 2020)

Factors	Precipitation	Slope	Flow Accumulation	DEM	Distance to River	Drainage Density	TWI	LULC	Distance from TRI	TRI density	NDVI
Precipitation	0.1500	0.2264	0.2581	0.0960	0.1481	0.1270	0.1440	0.1224	0.1224	0.0968	0.0882
Slope	0.0750	0.1132	0.1290	0.2880	0.1481	0.1905	0.1440	0.0612	0.0612	0.0968	0.0882
Flow Accumulation	0.0750	0.1132	0.1290	0.1920	0.1481	0.1905	0.1440	0.1224	0.1837	0.0968	0.1176
DEM	0.1500	0.0377	0.0645	0.0960	0.2222	0.1270	0.1440	0.1224	0.1224	0.0968	0.1176
Distance to River	0.0750	0.0566	0.0645	0.0320	0.0741	0.1270	0.1440	0.1837	0.0612	0.0968	0.0882
Drainage density	0.0750	0.0377	0.0430	0.0480	0.0370	0.0635	0.0960	0.1224	0.1224	0.0968	0.1176
TWI	0.0500	0.0377	0.0430	0.0320	0.0247	0.0317	0.0480	0.0612	0.1224	0.0968	0.0882
LULC	0.0750	0.1132	0.0645	0.0480	0.0247	0.0317	0.0480	0.0612	0.0612	0.0968	0.0882
Distance from TRI	0.0750	0.1132	0.0430	0.0480	0.0741	0.0317	0.0240	0.0612	0.0612	0.0968	0.0882
TRI density	0.1500	0.1132	0.1290	0.0960	0.0741	0.0635	0.0480	0.0612	0.0612	0.0968	0.0882
NDVI	0.0500	0.0377	0.0323	0.0240	0.0247	0.0159	0.0160	0.0204	0.0204	0.0323	0.0294

Table 3.7. Resulting weights of all criteria based on pairwise comparison (for 2000, 2010 and 2020).

Factors	Weight	Weight Percentage
Annual Average Precipitation	0.1436	14
Slope	0.1268	13
Flow Accumulation	0.1375	14
DEM	0.1183	12
Distance to River	0.0912	9
Drainage density	0.0781	8
TWI	0.0578	6
LULC	0.0648	6
Distance from TRI	0.0651	7
TRI density	0.0892	9
NDVI	0.0275	3

3.2.6 Reclassification of risk factors

In this study, a Multi-Criteria Decision Analysis (MCDA) approach necessitates the transformation and reclassification of raster datasets to ensure consistency and comparability when combining the different parameters. This is because the scale of the original raster values can vary greatly which can severely limit the impact that weights have on the final output. Therefore, all raster datasets (Table 3.2) for the years 2000, 2010, and 2020 have been transformed into reclassified values using the reclassify tool in ArcGIS Pro. This tool adjusts the input values from each dataset to fit within five classes, ranging from 1 to 5. The natural break (Jenks) classification method has been employed to group data, aiming to minimize the average deviation within each class while maximizing the deviation between classes. This approach reduces variance within classes and enhances it between them, thereby optimizing the classification (Jenks, 1967).

In this classification scheme, a value of 1 indicates a minimal potential risk of flooding, whereas a value of 5 signifies a heightened risk. For parameters such as Rainfall, Topographic Wetness Index (TWI), Flow Accumulation, and Drainage Density, an increase in value corresponds

to an increased flood potential, indicating higher risks with rising values of these parameters. Conversely, for parameters like Digital Elevation Model (DEM), Slope, Distance from the Primary River, Land Use Land Cover (LULC), and Normalized Difference Vegetation Index (NDVI), an increase in value correlates with a decrease in flood potential, signifying lower risks with higher values of these parameters.

Additionally, for parameters such as Toxic Release Inventory (TRI) density and Distance from TRI, reclassification is crucial due to their role in contaminating floodwaters rather than directly influencing flood potential. An increase in TRI density corresponds to a higher risk of contamination, while an increased distance from TRI sites correlates with a lower contamination risk.

The reclassification procedure normalizes all datasets representing the risk sources into a common scale from 1 to 5 (Table 3.8). Once scaled, weights can be applied to adjust for the importance of each dataset (as determined by the AHP), as well as evaluate different scenarios when certain risk factors are more influential than others. This enables a more nuanced assessment of flood risk that considers the varying influence that different geographical and environmental parameters may have on flooding and contamination over space and time.

Table 3.8: Classes of the flood vulnerability factors used in the study and their ratings (for 2000, 2010 and 2020)

Parameters	**Year**					
	2000		**2010**		**2020**	
	Class	**Rating**	**Class**	**Rating**	**Class**	**Rating**
Digital Elevation Model (DEM) (m)	24.30 - 129.15	5	24.30 - 129.15	5	24.30 - 129.15	5
	129.15 - 195.78	4	129.15 - 195.78	4	129.15 - 195.78	4
	195.78 - 277.42	3	195.78 - 277.42	3	195.78 - 277.42	3
	277.42 - 385.54	2	277.42 - 385.54	2	277.42 - 385.54	2
	385.54 - 633.31	1	385.54 - 633.31	1	385.54 - 633.31	1
Slope (degree)	0- 3.35	5	0- 3.35	5	0- 3.35	5
	3.35 - 7.55	4	3.35 - 7.55	4	3.35 - 7.55	4
	7.55 - 12.90	3	7.55 - 12.90	3	7.55 - 12.90	3

	12.90 - 20.23	2	12.90 - 20.23	2	12.90 - 20.23	2
	20.23 - 77.73	1	20.23 - 77.73	1	20.23 - 77.73	1
Flow Accumulation	0 - 31375153	1	0 - 31375153	1	0 - 31375153	1
	31375153 - 92631404	2	31375153 - 92631404	2	31375153 - 92631404	2
	92631404 - 146417380	3	92631404 - 146417380	3	92631404 - 146417380	3
	146417380 7 - 200203356	4	146417380 7 - 200203356	4	146417380 7 - 200203356	4
	200203356 - 380984000	5	200203356 - 380984000	5	200203356 - 380984000	5
Precipitation (mm)	825 - 985	1	1033 - 1152	1	1406 - 1589	1
	985 - 1056	2	1152 - 1219	2	1589 - 1690	2
	1056 - 1126	3	1219 - 1285	3	1690 - 1804	3
	1126 - 1213	4	1285 - 1356	4	1804 - 1930	4
	1213 - 1494	5	1356 - 1523	5	1930 - 2165	5
Land Use / Land Cover (LULC)	Deciduous, Evergreen, Mixed Forest, Shrub/Scrub	1	Deciduous, Evergreen, Mixed Forest, Shrub/Scrub	1	Deciduous, Evergreen, Mixed Forest, Shrub/Scrub	1
	Developed Areas (Open Space and Low Intensity), Barren Land (Rock/Sand/Clay	2	Developed Areas (Open Space and Low Intensity), Barren Land (Rock/Sand/Clay	2	Developed Areas (Open Space and Low Intensity), Barren Land (Rock/Sand/Clay	2
	Developed Areas (Medium and High Intensity)	3	Developed Areas (Medium and High Intensity)	3	Developed Areas (Medium and High Intensity)	3
	Grassland/Herbaceous, Pasture/Hay	4	Grassland/Herbaceous, Pasture/Hay	4	Grassland/Herbaceous, Pasture/Hay	4

	Open Water, Cultivated Crops, Woody Wetlands	5	Open Water, Cultivated Crops, Woody Wetlands	5	Open Water, Cultivated Crops, Woody Wetlands	5
Distance from the main river (m)	0 - 1835	5	0 - 1835	5	0 - 1835	5
	1835 - 4057	4	1835 - 4057	4	1835 - 4057	4
	4057 - 6569	3	4057 - 6569	3	4057 - 6569	3
	6569 - 10048	2	6569 - 10048	2	6569 - 10048	2
	10048 - 24637	1	10048 - 24637	1	10048 - 24637	1
Topographic Wetness Index (TWI)	0.66 - 4.36	1	0.66 - 4.36	1	0.66 - 4.36	1
	4.36 - 5.64	2	4.36 - 5.64	2	4.36 - 5.64	2
	5.64 - 7.55	3	5.64 - 7.55	3	5.64 - 7.55	3
	7.55 - 11.96	4	7.55 - 11.96	4	7.55 - 11.96	4
	11.96 - 19.39	5	11.96 - 19.39	5	11.96 - 19.39	5
Normalized Difference Vegetation Index (NDVI)	-0.61 - 0.03	5	-0.63 - 0.05	5	-0.191 - -0.01	5
	0.03- 0.36	4	0.05 - 0.35	4	-0.01 - 0.35	4
	0.36 - 0.53	3	0.35 - 0.51	3	0.35 - 0.56	3
	0.53 - 0.66	2	0.51 - 0.64	2	0.56 - 0.71	2
	0.67 - 0.86	1	0.64 - 0.88	1	0.71 - 0.93	1
Distance from TRI (m)	0 - 12979	5	0 - 12979	5	0 - 15149	5
	12979 - 23055	4	12979 - 23055	4	15149 - 26164	4
	23055 - 34122	3	23055 - 34122	3	26164 - 38015	3
	34122 - 47969	2	34122 - 47969	2	38015 - 54508	2
	47969- 72512	1	47969 - 72512	1	54508 - 83381	1
TRI density (pounds/ Sq. Km)	0 - 91	1	0 - 303	1	0 - 794	1
	91 - 321	2	303 - 1345	2	794 - 3116	2
	321 - 695	3	1345 - 2923	3	3116 - 6364	3
	695 - 1189	4	2923 - 4669	4	6364 - 9930	4
	1189 - 1719	5	4669 - 6535	5	9930 -13724	5
Drainage density	0.000272 - 0.000625	1	0.000272 - 0.000625	1	0.000272 - 0.000625	1

(km/km)	0.000625 - 0.000833	2	0.000625 - 0.000833	2	0.000625 - 0.000833	2
	0.000833 - 0.001082	3	0.000833 - 0.001082	3	0.000833 - 0.001082	3
	0.001082 - 0.001377	4	0.001082 - 0.001377	4	0.001082 - 0.001377	4
	0.001377 - 0.001748	5	0.001377 - 0.001748	5	0.001377 - 0.001748	5

3.3.7 Weighted Overlay analysis for generating final flood risk and contamination likelihood map

Weighted Overlay is a spatial analysis technique used to combine multiple raster layers, into a single output layer. This process involves standardizing the input values, assigning weights to each layer based on their relative importance, and summing the weighted values to identify the optimal or high-risk areas (Guntara, I., 2013).

Each of the compound hazard criteria layers detailed previously were reclassified from 1-5 (Table 3.8). The final compound hazard maps have been generated by multiplying each layer by its respective weight (determined by the AHP method) and adding all the weighted layers together (Table 3.7). This weighted overlay approach is one method of modeling suitability/vulnerability. The Weighted Overlay is represented mathematically using the equation 14:

$$Weighted\ Overlay = \Sigma\ (Xi * Wi) \qquad (14)$$

where Xi is the cell value of raster and Wi is the corresponding weight. Finally, a compound hazard risk map was generated by considering the block groups within the Coosa River watershed. The average values were calculated using the 'Zonal Statistics as Table' tool to delineate the likelihood of contamination within the watershed for each block group. This analysis identified the block groups with varying levels of the likelihood of contamination due to flooding, categorizing them as low, moderately low, medium, moderately high, and high risk.

3.3.8 Exploratory spatial analysis: Bivariate Local Moran's I

The compound hazard risk maps were assessed using a bivariate Local Indicators of Spatial Association (LISA) statistic to conduct an exploratory spatial analysis between the contaminated flood water exposure areas and social vulnerability indices for the years 2000, 2010 and 2020 across different tracts of block groups in the Coosa River watershed. Essentially, bivariate LISA maps provide a spatial representation of how the value of one variable (contaminated flood water exposure) is geographically surrounded by the values of a second variable (social vulnerability index).

The statistical method identifies two forms of spatial interdependence - positive spatial autocorrelation (clustering) and negative spatial autocorrelation (dispersity). Positive spatial autocorrelation is observed when high values of flood exposure coincide geographically with high values of social vulnerability (creating High-High hotspots) or when low values of flood risk are surrounded by low values of the other (forming Low-Low cold spots). On the other hand, negative spatial autocorrelation is characterized by the juxtaposition of high and low values leading to High-Low or Low-High clusters (Tate et. al, 2021), commonly referred to as spatial outliers.

This use of bivariate Local Moran's I offers an understanding of how regions with high contaminated flood exposure overlap with areas of high social vulnerability. However, it's important to note that while LISA statistics excel in identifying spatial clusters and formulating hypotheses, they do not elucidate the causal mechanisms that may underlie these spatial relationships. The significance of each cluster is statistically determined by comparing the observed local spatial patterns against a reference distribution generated through random permutations of the data, as performed in Bivariate Local Moran's I analysis. This analysis also produces a global spatial autocorrelation statistic, averaging local values, for the entire area under study (Anselin, 1995). GeoDa has been used to perform the Bivariate Local Moran's I analysis for the years 2000, 2010 and 2020.

4. Results

4.1 Toxic chemical release trends from TRI facilities

One of the more influential factors in determining where and to what extent contaminatned flood waters may impact surrounding communities is the amount of pollution being released by TRI facilities. Therefore, the total quantity of toxic chemicals released to air, water, and land onsite from TRI facilities was analyzed to observe the trend of these releases over the period from 2000 to 2020 for those areas within the studies extent.

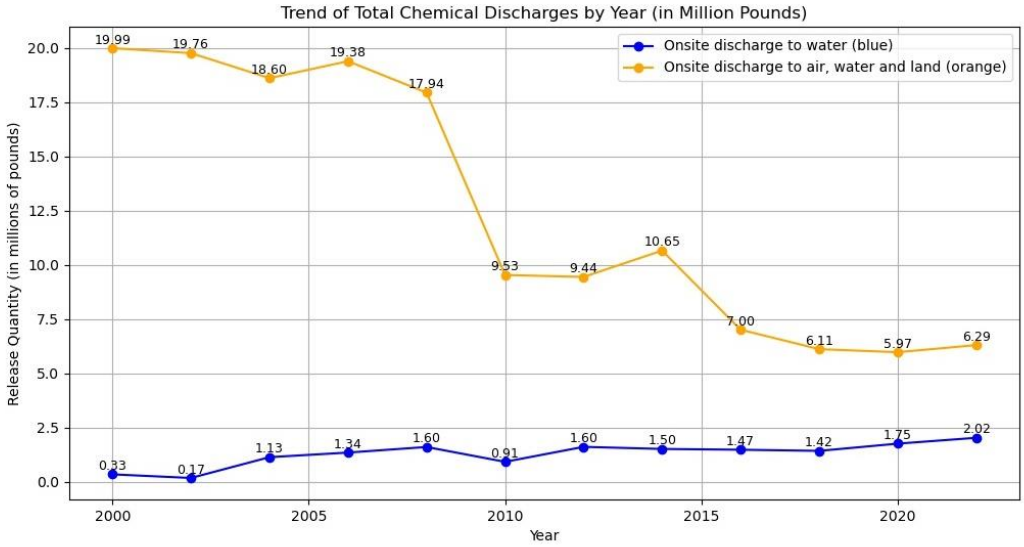

Figure 4.1: Trend of total chemical discharge from toxic release inventory (TRI) facilities (2-year interval from 2000 to 2022) in million pounds.

Figure 4.1 illustrates the total onsite chemical discharges to surface water (blue line) and the aggregate onsite release of toxic chemicals to air, water, and land (orange line) from 2000 to 2022, measured in millions of pounds. The data reveals a relatively stable yet gradually increasing trend in onsite discharges to surface water. Starting at about 0.33 million pounds in 2000, the discharge values fluctuate slightly over the years, reaching 1.75 million pounds in 2020 and peaking at 2.02 million pounds in 2022. Conversely, the total quantity of chemicals released onsite to air, water, and land shows a significant decline over the same period. Initially, the releases were at 19.99 million pounds in 2000, with a slight peak at 19.76 million pounds in 2002. After this peak, the trend follows a downward trajectory, with intermittent fluctuations, reaching 5.97 million pounds in 2020, and eventually reaching 6.29 million pounds by 2022.

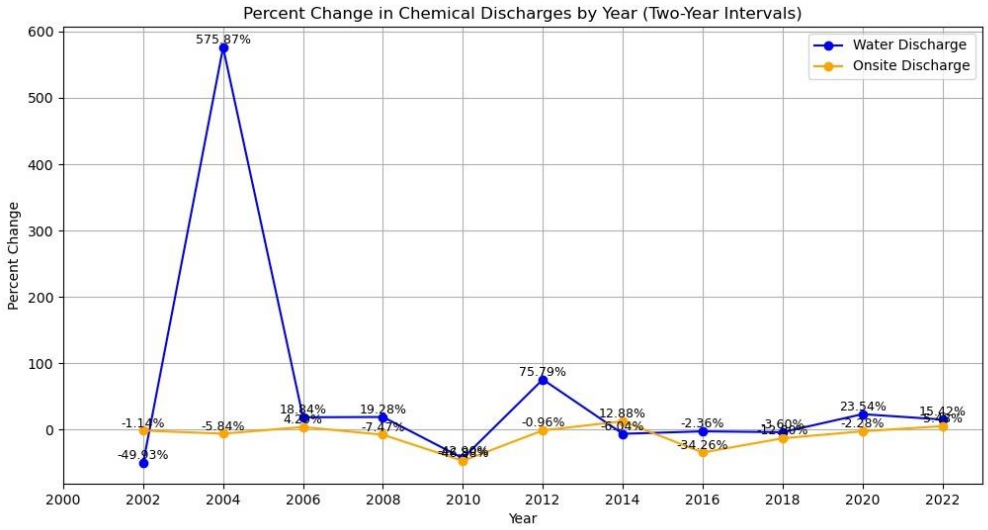

Figure 4.2: Percent change in chemical discharge from toxic release inventory (TRI) facilities (2-year interval from 2000 to 2022)

Figure 4.2 presents the percentage change in total onsite chemical discharges to surface water and the total quantity of toxic chemicals released to air, water, and land, examined in two-year intervals from 2000 to 2022.

The graph captures volatility in both categories, with stark fluctuations that reflect underlying shifts in industrial practices and regulatory impacts. Particularly, the percentage change in water discharge is characterized by dramatic oscillations. A surge of 575.87% in 2004 marks the most pronounced spike, pointing out a period of significant increase in waterborne chemical discharges. Subsequent years exhibit moderate fluctuations, with another peak of 75.79% observed in 2012, followed by a rise of 23.54% in 2020.

In contrast, the total onsite discharge of toxic chemicals to air, water, and land reveals a more tempered pattern of variation. The percentage changes in this category demonstrate less severe oscillations, characterized by a peak increase of 19.28% in 2006, juxtaposed with a substantial decrease of 34.26% in 2016.

4.1.1 Chemical emissions:

Figure 4.3 elucidates the total quantity of chemicals (top 15) released to water in 2000, 2010, and 2020, presented on a logarithmic scale and measured in millions of pounds. This

temporal analysis highlights significant shifts in the magnitude and composition of chemical discharges over the two-decade span.

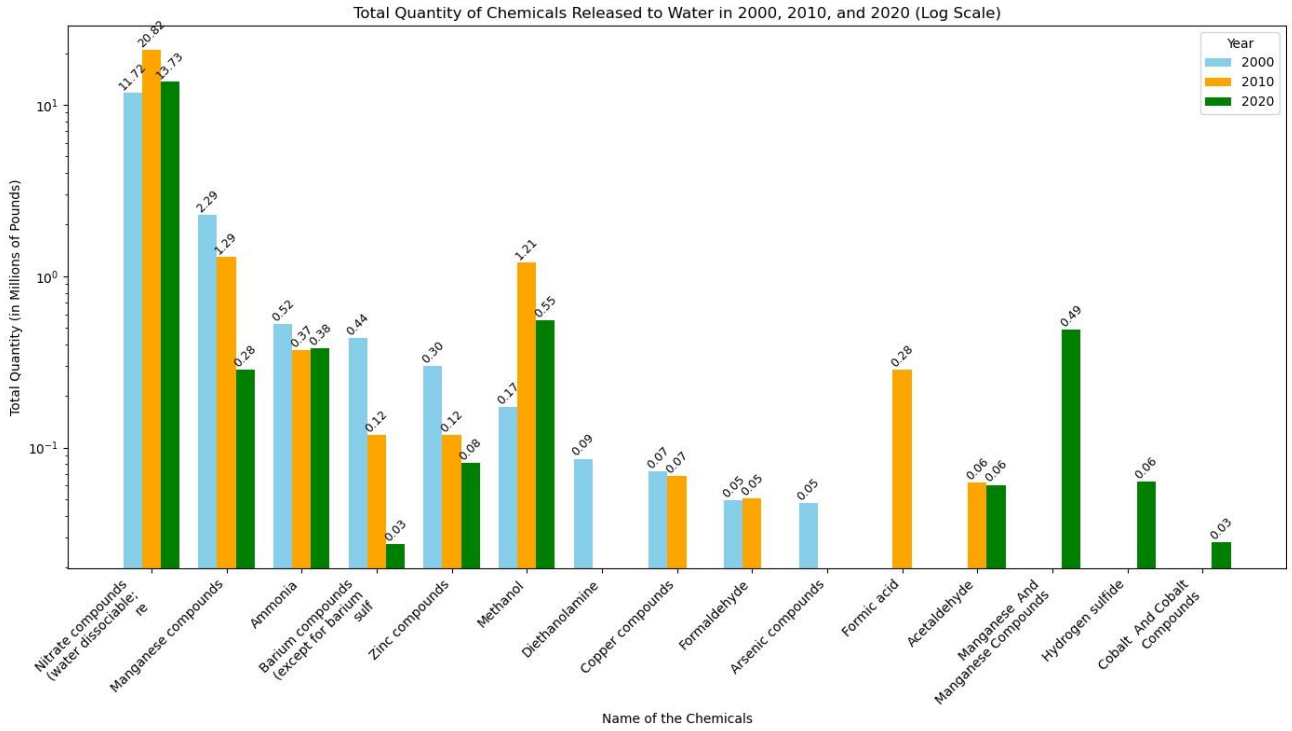

Figure 4.3: Total quantity of chemicals (top 15) released from toxic release inventory (TRI) facilities for the years 2000, 2010 and 2020.

In the year 2000, the highest quantities of chemicals released to water were Nitrate Compounds and Zinc Compounds, with releases amounting to approximately 1510.27 thousand pounds and 782.84 thousand pounds, respectively. These chemicals were followed by Barium Compounds (135.97 thousand pounds) and Manganese Compounds (65.29 thousand pounds). The data also shows significant releases of Ammonia (28.69 thousand pounds), with Ethylene Glycol and Copper Compounds contributing 10.79 and 8.30 thousand pounds respectively. Smaller quantities of chemicals such as Arsenic Compounds (23.48 thousand pounds), Methanol (9.35 thousand pounds), and Vanadium Compounds (3.00 thousand pounds) were also reported.

A decade later, in 2010, there were notable changes in the quantities of chemicals released. Nitrate Compounds continued to be the most substantial emission, with a significant increase to 1570.27 thousand pounds. Zinc Compounds also saw an increase to 961.24 thousand pounds. Conversely, Barium Compounds decreased to 64.96 thousand pounds, while Manganese

Compounds slightly decreased to 43.76 thousand pounds. Ammonia showed a reduction to 19.67 thousand pounds. Interestingly, certain chemicals such as Methanol exhibited a considerable increase to 11.14 thousand pounds, whereas the release of Vanadium Compounds decreased to 1.75 thousand pounds. New chemicals such as Diethanolamine and Nonylphenol Ethoxylates appeared in the data, with releases of 3.00 and 1.14 thousand pounds, respectively.

By 2020, the trend of chemical releases displayed further variability. Nitrate Compounds reached their highest recorded level at 1570.27 thousand pounds. Zinc Compounds remained significant at 782.84 thousand pounds. However, there were decreases in the release of other chemicals such as Barium Compounds (9.87 thousand pounds) and Ammonia (3.53 thousand pounds). Manganese Compounds and Ethylene Glycol releases were also reduced to 43.76 and 10.79 thousand pounds respectively. Notably, new chemicals such as Nonylphenol Ethoxylates had an increased release of 5.15 thousand pounds, while Methanol saw a reduction to 1.14 thousand pounds.

The analysis of the data from 2000 to 2020 reveals significant trends in the release of chemicals to water. Nitrate Compounds consistently represented the highest quantity of emissions across all three years, with substantial increases over time. Zinc Compounds also showed a significant upward trend. Conversely, some chemicals, such as Barium Compounds and Ammonia, exhibited a decrease in release quantities over the years.

4.1.2 Emission industries:

In addition to the total emissions and emissions by chemical, the TRI data also reports emissions by industry. Figures 4.4, 4.5, and 4.6 illustrate the industry sectors responsible for the release of the top 15 chemicals, in terms of discharge quantity, to the Coosa River watershed for the years 2000, 2010, and 2020, respectively. This approach allows for a clearer comparison across chemicals with vastly differing emission sources.

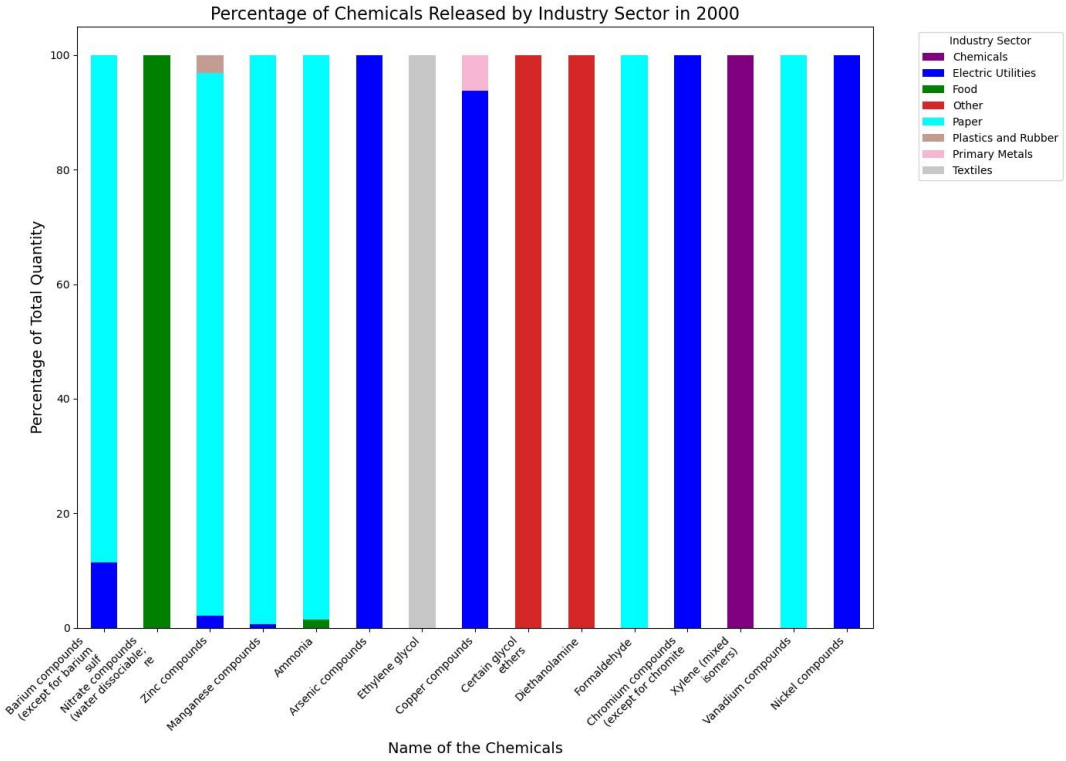

Figure 4.4: Types of industry sectors (TRI facilities) releasing chemicals (top 15) in 2000.

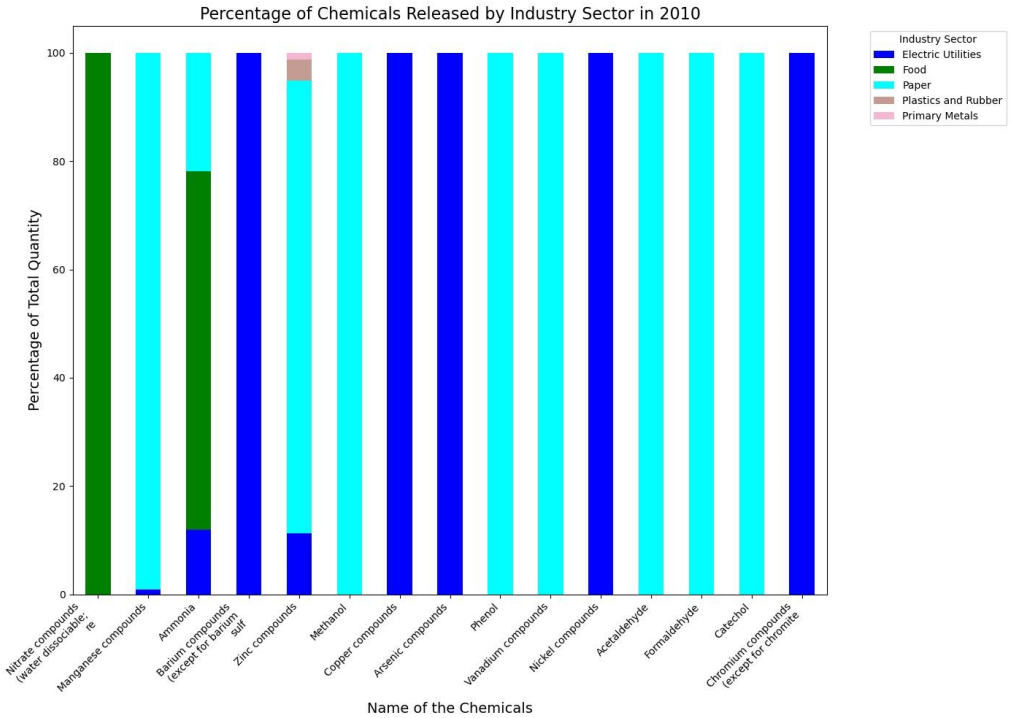

Figure 4.5: Types of industry sectors (TRI facilities) releasing chemicals (top 15) in 2010.

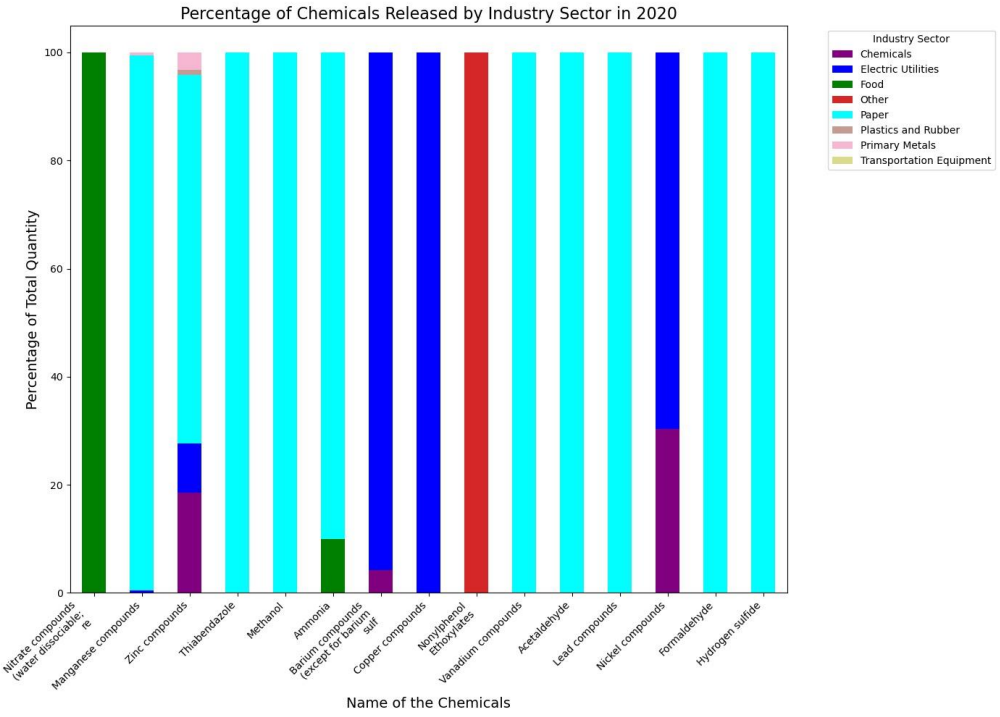

Figure 4.6: Types of industry sectors (TRI facilities) releasing chemicals (top 15) in 2020.

In 2000 (Figure 4.4), the food industry was predominantly responsible for the release of nitrate compounds, as indicated by the green bar in the provided graph. The paper industry, represented by cyan bars, emerged as a significant source of multiple chemicals, including ammonia, manganese compounds, and methanol. Concurrently, electric utilities, denoted by blue bars, were major contributors to the discharge of arsenic, barium, and chromium compounds. A decade later in 2010 (Figure 4.5), the paper industry maintained its status as a major polluter, continuing to discharge substantial amounts of ammonia, manganese compounds, and zinc compounds. The food industry sustained its role as the leading emitter of nitrate compounds. Electric utilities remained prominent in releasing arsenic, barium, chromium, and copper compounds into surface water. Additionally, new sectors such as fabricated metals and nonmetallic mineral products began to emerge as more prominent sources of chemical emissions. By this time, the spectrum of emitters had broadened to include manufacturers of electrical equipment, wood

products, and chemicals, indicating a diversification in the industrial contributors to chemical pollution.

By 2020 (Figure 4.6), the paper industry continued to be a significant contributor to chemical releases, particularly ammonia and manganese compounds. The food industry consistently discharged nitrate compounds, maintaining its pivotal role as a key emitter. Electric utilities persisted in their emissions of zinc and nickel compounds. Furthermore, the transportation equipment sector emerged as a notable contributor to the release of various chemicals, marking a shift in the industrial landscape of chemical emissions. This period also saw the addition of sectors such as petroleum, textiles, plastics and rubber, contributing to the expanding array of industrial sources of chemical discharges.

4.1.3 Distribution of TRI facilities in the Coosa River watershed:

Table 4.1: Total no. of toxic release inventory (TRI) facilities located in the Coosa River watershed (2000 – 2020).

Year	No. of TRIs that release chemicals to land, water and Air (≥ 100 pounds)	No. of TRIs that release chemicals to surface water (≥ 100 pounds)	Percentage of total TRIs that release chemicals to surface water
2000	184	37	20.10
2002	184	27	14.67
2004	191	37	19.37
2006	192	35	18.22
2008	182	37	20.32
2010	185	41	22.16
2012	168	37	22.02
2014	180	35	19.44
2016	165	32	19.39
2018	169	34	20.11
2020	160	33	20.62

Table 4.1 offers a detailed account of the total number of TRI facilities within the Coosa River watershed from 2000 to 2020, delineating those that release chemicals to land, water, and air (≥ 100 pounds) as well as those specifically discharging to surface water. In 2000, there were 184 TRI facilities releasing significant quantities of chemicals to land, water, and air. This number experienced fluctuations over the years, peaking at 192 facilities in 2006 and ultimately declining to 160 facilities by 2020. The number of TRI facilities discharging chemicals to surface water also demonstrated variability. In 2000, 37 facilities were reported to release chemicals to surface water, reaching a peak of 41 facilities in 2010 and then stabilizing at 33 facilities by 2020. The percentage of total TRI facilities that released chemicals to surface water, shown in the last column, provides further insight into these trends. Starting at 20.10% in 2000, the percentage saw a decrease to 14.67% in 2002, followed by periods of gradual increase and stabilization, reaching 20.62 % in 2020.

4.1.4 Emerging hotspot analysis of the TRI facilities (from 2000 to 2020)

The Emerging Hotspot Analysis map for the Coosa River watershed, spanning from 2000 to 2020, provides a visualization of the spatial and temporal dynamics of TRI facilities' discharges. This analysis identifies several critical areas within the watershed, highlighting regions of persistent and emerging environmental concern.

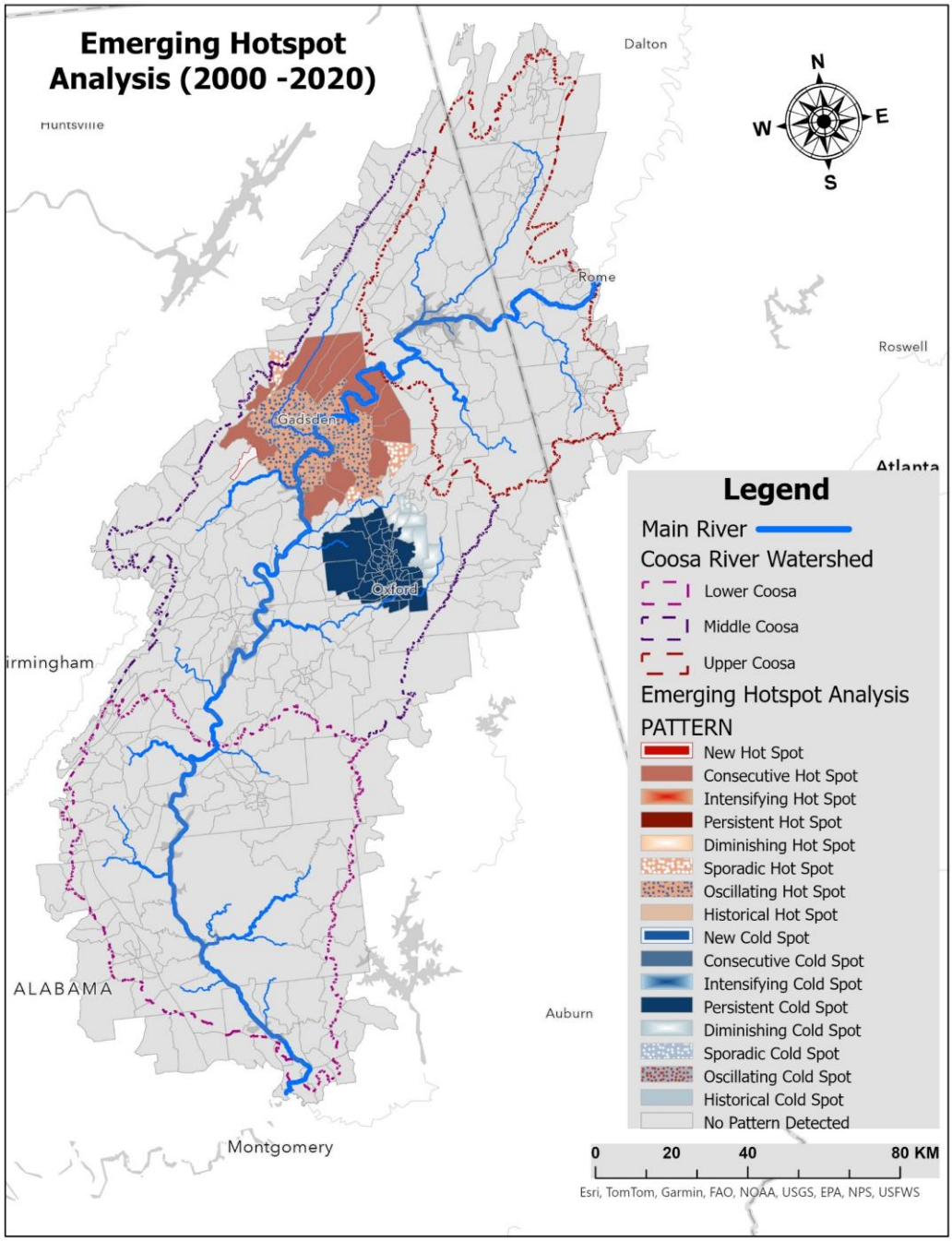

Figure 4.7: Map Showing the Results of the Emerging Hotspot Analysis of the toxic release inventory (TRI) facilities for the Years 2000 to 2020 revealing patterns.

Table 4.2: Patterns Observed in the Emerging Hotspot Analysis (2000 – 2020) and Percentage of Areas for Each Category

Patterns observed	**Percentage of area (%)**
Consecutive Hot Spot	3.27
Diminishing Cold Spot	0.63
New Hot Spot	0.07
No Pattern Detected	90.4
Oscillating Hot Spot	2.82
Persistent Cold Spot	2.28
Sporadic Hot Spot	0.42

The results, depicted in Figure 4.7 and Table 4.2, reveal that consecutive hotspots, which encompass 3.27% of the area, denote regions that have consistently endured high levels of TRI discharges over the years. These areas are predominantly situated in the upper and middle sections of the watershed, particularly around Gadsden. Diminishing cold spots, representing 0.63% of the area, indicate regions where TRI discharges have abated over time. Conversely, new hotspots, although accounting for a mere 0.07% of the area, signify emergent areas that have recently begun experiencing elevated levels of discharges.

Adjacent to the Gadsden area, several regions are marked by sporadic hotspots, which encompass 0.42% of the area. These regions exhibit irregular occurrences of high discharge levels. A significant portion of the watershed, particularly in the lower Coosa region, is characterized by the absence of any discernible pattern, as indicated by the grey areas covering 90.4% of the area. In the middle Coosa region, around Oxford, the analysis reveals the presence of both oscillating and persistent cold spots. Oscillating hotspots, covering 2.82% of the area and shown in orange, represent regions with fluctuating discharge levels. Persistent cold spots, comprising 2.28% of the area and indicated by dark blue, denote regions with consistently low discharge levels.

4.2 Social vulnerability in the Coosa River watershed

The analysis of the Social Vulnerability Index (SoVI) data for communities within the counties in the Coosa River watershed over the years 2000, 2010, and 2020 provides insights into the changing socio-economic conditions that may make these communities more vulnerable to the impact of flooding and contamination. The SoVI ranges from 0 to 1. For the sake of clarity, the SoVI of the block groups within the study area have been grouped into five categories: low (≤ .2), moderately low (≤ .4), moderate (≤ .6), and moderately high (≤ .8) and high (≤ 1) (Table 4.2). By examining the SoVI for block groups within the watershed across these years, trends and patterns in social vulnerability can be identified and interpreted. The spatial distribution of the SoVI and the number of block groups falling into each of the bins is presented in Figure 4.8 (A, B and C) and in Table 4.3.

Table 4.3: Distribution of block groups by social vulnerability index (SoVI) categories in different years (for 2000, 2010 and 2020)

Year	River Segment	Low (%)	Moderately Low (%)	Moderate (%)	Moderately High (%)	High (%)
2000	Upper Coosa	17.15	51.44	25.72	5.69	0
	Middle Coosa	21.06	52.32	22.50	4.12	0
	Lower Coosa	9.34	54.29	23.85	0.22	12.30
	Total Coosa watershed	15.41	54.05	23.26	4.29	2.98
2010	Upper Coosa	0	68.73	28.56	2.71	0
	Middle Coosa	3.48	55.90	35.18	5.00	0.43
	Lower Coosa	0.05	65.15	33.58	1.22	0
	Total Coosa watershed	1.29	61.22	34.05	3.02	0.39
2020	Upper Coosa	44.20	42.54	13.06	0.20	0
	Middle Coosa	18.58	60.63	16.90	3.89	0
	Lower Coosa	22.37	56.59	16.22	4.17	0.65
	Total Coosa watershed	24.76	54.96	17.37	2.75	0.16

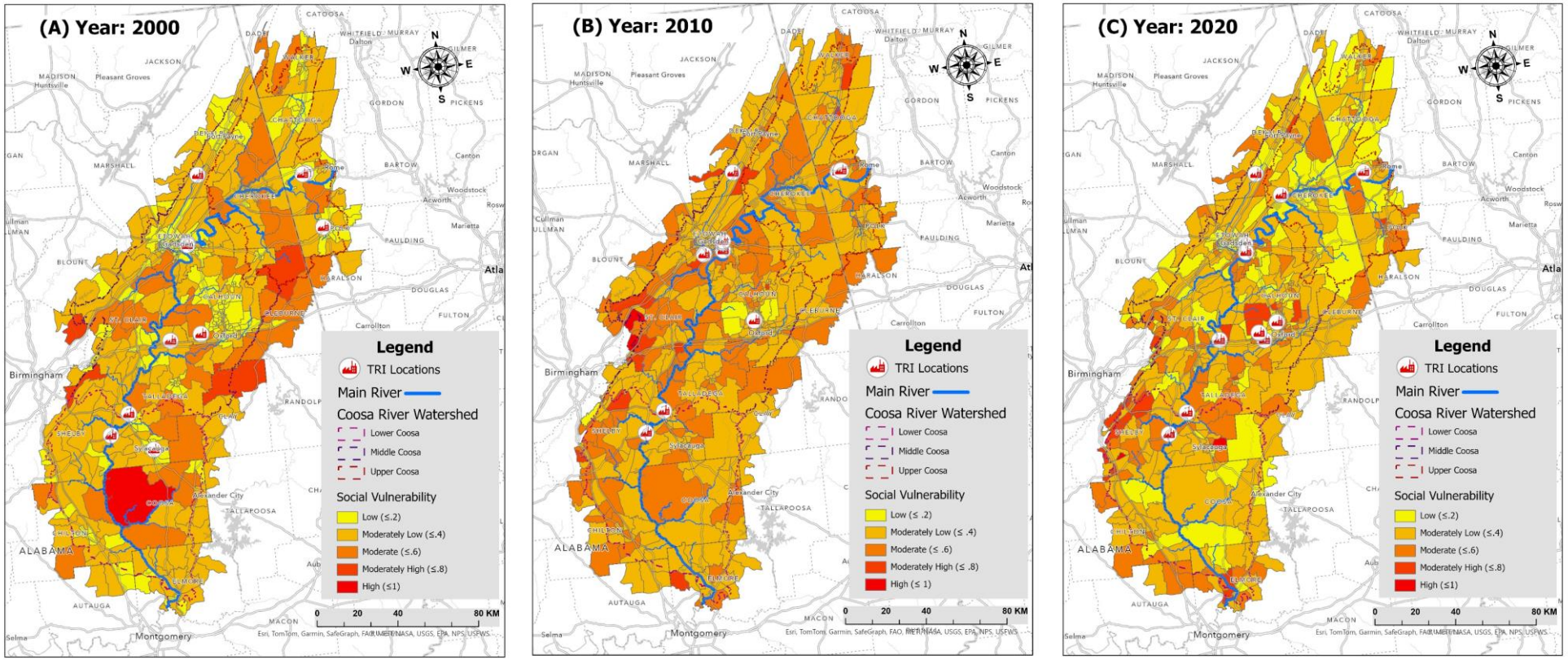

Figure 4.8: Social vulnerability map of Coosa River watershed for the years 2000, 2010 and 2020.

In the year 2000 (Figure 4.8 A and Table 4.3) In the upper Coosa region, areas such as Rome and the surrounding vicinity displayed a majority of block groups with low to moderately low social vulnerability. Specifically, 17.15% of the block groups fell into the low vulnerability category, and 51.44% were categorized as moderately low vulnerability. Moving towards the middle Coosa region, including places like Gadsden and Oxford, there is an evident increase in social vulnerability. This region exhibited higher proportions of block groups with moderate to moderately high vulnerability, with 25.72% of block groups classified as moderate and 5.69% as moderately high vulnerability. These areas, marked in orange and red on the map, highlight socio-economic challenges that potentially increase their susceptibility to environmental and industrial hazards. In the lower Coosa region, the social vulnerability profile is diverse. Here, 9.34% of the block groups were categorized as low vulnerability, and 54.29% fell into the moderately low category. However, there is also a noticeable presence of higher vulnerability, with 23.85% of block groups classified as moderate and 12.30% as high vulnerability shown in dark red.

In 2010 (Figure 4.8 B and Table 4.3), the upper Coosa region experienced a significant change in social vulnerability. Specifically, 68.73% of the block groups were categorized as moderately low vulnerability, a marked increase indicating some socio-economic improvements in this region. Conversely, the middle Coosa region, including areas such as Etowah and St. Clair counties, saw an increase in moderate to moderately high vulnerability. In this segment, 3.48% of the block groups were classified as low vulnerability, 55.90% as moderately low, and 35.18% as moderate. This represents a shift towards higher vulnerability compared to the year 2000. The lower Coosa region displayed similar trends, with 65.15% of the block groups categorized as moderately low and 33.58% as moderate vulnerability. This region also showed a small percentage (1.22%) of block groups in the moderately high vulnerability category, reflecting ongoing socio-economic pressures despite some areas showing improvements. Overall, for the entire Coosa River watershed in 2010, 1.29% of the block groups were categorized as low vulnerability, 61.22% as moderately low, and 34.05% as moderate. The moderately high vulnerability category comprised 3.02% of the watershed, with 0.39% categorized as high vulnerability.

In 2020 (Figure 4.8 C and Table 4.3), the upper Coosa region exhibited a notable increase in block groups with low vulnerability, rising to 44.20% from 0% in 2010 and 17.15% in 2000. The proportion of block groups with moderately low vulnerability decreased to 42.54% compared

to 68.73% in 2010, reflecting an overall positive shift towards lower vulnerability categories. The middle Coosa region also showed improvements, with 18.58% of block groups classified as low vulnerability, up from 3.48% in 2010 and 21.06% in 2000. The percentage of moderately low vulnerability block groups increased slightly to 60.63%, while moderate vulnerability decreased to 16.90%. The lower Coosa region demonstrated significant changes as well. The percentage of block groups with low vulnerability increased to 22.37% from 0.05% in 2010 and 9.34% in 2000. The proportion of moderately low vulnerability block groups rose to 56.59%, while moderate vulnerability decreased to 16.22%. Overall, for the entire Coosa River watershed in 2020, 24.76% of block groups were categorized as low vulnerability, a substantial increase from 1.29% in 2010 and 15.41% in 2000. The moderately low vulnerability category comprised 54.96% of the watershed, showing stability compared to 54.05% in 2000 and 61.22% in 2010. The moderate vulnerability category decreased to 17.37% from 34.05% in 2010 and 23.26% in 2000. The percentage of block groups with moderately high vulnerability dropped to 2.75% from 3.02% in 2010, and high vulnerability significantly decreased to 0.16% from 2.98% in 2000 and 0.39% in 2010.

4.3 Likelihood of contamination associated with flood risk areas in the Coosa River watershed

Figure 4.9 presents the maps depicting the likelihood of contamination associated with flood risk in the Coosa River watershed. The maps were generated by multiplying each layer by its respective weight (determined by the AHP method) and summing all the weighted layers together. All block groups within the watershed are shown in the maps for the years 2000, 2010, and 2020. Each map categorizes areas into five risk levels: low (≤ .2), moderately low (≤ .4), moderate (≤ .6), and moderately high (≤ .8) and high (≤ 1) (Table 4.4).

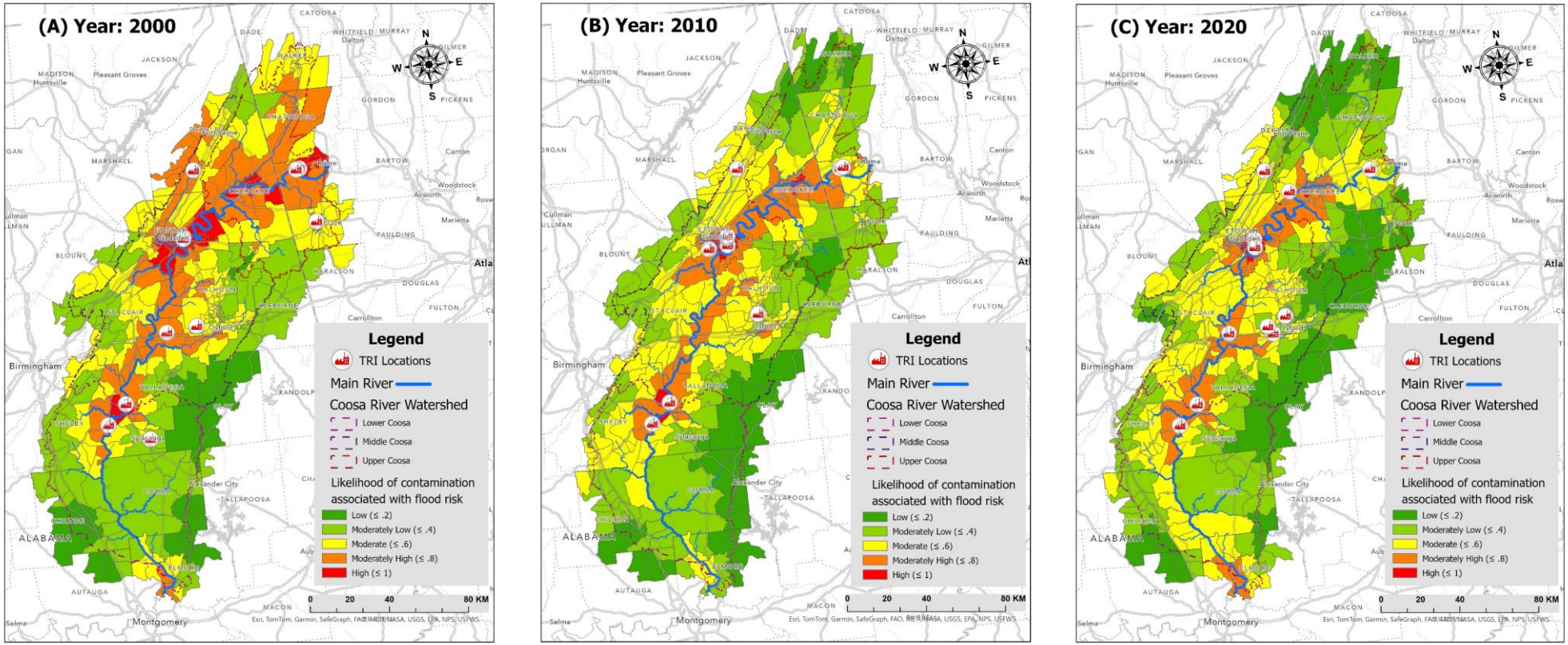

Figure 4.9: Likelihood of contamination associated with flood risk map of Coosa River watershed for the years 2000, 2010 and 2020.

Table 4.4: Spatial distribution of block groups by Likelihood of contamination associated with flood risk categories in different years (for 2000, 2010 and 2020)

Year	River Segment	Low (%)	Moderately Low (%)	Moderate (%)	Moderately High (%)	High (%)
2000	Upper Coosa	1.37	12.61	37.66	42.64	5.72
	Middle Coosa	5.80	24.62	35.62	26.46	7.50
	Lower Coosa	15.59	61.50	15.58	5.89	1.44
	Total Coosa watershed	12.42	33.18	29.37	20.98	4.05
2010	Upper Coosa	14.57	35.90	30.52	18.27	0.74
	Middle Coosa	6.13	20.47	45.97	24.92	2.50
	Lower Coosa	21.05	48.93	24.43	5.05	0.53
	Total Coosa watershed	17.98	39.63	29.86	11.45	1.08
2020	Upper Coosa	30.36	32.48	26.29	10.62	0.26
	Middle Coosa	14.54	22.36	44.69	16.81	1.61
	Lower Coosa	11.55	46.21	33.44	8.80	0
	Total Coosa watershed	24.39	33.66	31.30	10.07	0.57

In 2000 (Figure 4.9 A and Table 4.4), the upper Coosa region, including areas such as Walker, Rome, DeKalb, and Chattooga counties, exhibited a notable proportion of block groups categorized as having a moderate to high likelihood of contamination associated with flood risk. Specifically, 1.37% of the block groups were categorized as low risk, 12.61% as moderately low, 37.66% as moderate, 42.64% as moderately high, and 5.72% as high risk.

The middle Coosa region, including areas such as Cherokee and Etowah counties, also showed significant environmental risk. In this segment, 5.80% of the block groups were classified as low risk, 24.62% as moderately low, and 35.62% as moderate. Additionally, 26.46% were categorized as moderately high risk, and 7.50% as high risk.

The lower Coosa region, including areas such as Talladega, Shelby, and Elmore counties, displayed a different risk profile, with a higher percentage of block groups categorized as having a low to moderately low likelihood of contamination. Specifically, 15.59% of the block groups

were classified as low risk, 61.50% as moderately low, and 15.58% as moderate. The moderately high and high-risk categories comprised 5.89% and 1.44% of the block groups, respectively.

Overall, for the entire Coosa River watershed in 2000, 12.42% of the block groups were categorized as low risk, 33.18% as moderately low, and 29.37% as moderate. The moderately high-risk category comprised 20.98% of the watershed, with 4.05% categorized as high risk.

In 2010 (Figure 4.9 B and Table 4.4), the percentage of block groups in the upper Coosa region categorized as low risk increased significantly to 14.57% from 1.37% in 2000, indicating improved conditions. In areas such as Cherokee County, moderately low risk block groups also increased to 35.90% from 12.61%, while moderate risk decreased to 30.52% from 37.66%. The proportion of block groups in the moderately high-risk category dropped to 18.27% from 42.64%, and high risk decreased substantially to 0.74% from 5.72%.

The middle Coosa region, which includes places like Etowah and St. Clair counties, showed mixed results. The percentage of block groups categorized as low risk slightly increased to 6.13% from 5.80% in 2000. However, moderately low risk block groups decreased to 20.47% from 24.62%. The proportion of moderate risk block groups increased to 45.97% from 35.62%, while moderately high risk increased to 24.92% from 26.46%. High risk block groups saw a decrease to 2.50% from 7.50%.

The lower Coosa region, including counties such as Talladega and Shelby, also displayed significant changes. The percentage of block groups categorized as low risk increased to 21.05% from 15.59% in 2000, and moderately low risk decreased to 48.93% from 61.50%. The proportion of moderate risk block groups increased to 24.43% from 15.58%, suggesting heightened attention to areas previously considered low risk. Moderately high-risk block groups decreased to 5.05% from 5.89%, and high risk dropped to 0.53% from 1.44%.

In general, for the entire Coosa River watershed in 2010, 17.98% of the block groups were categorized as low risk, a significant increase from 12.42% in 2000. The moderately low risk category comprised 39.63% of the watershed, up from 33.18%. The proportion of moderate risk block groups remained relatively stable at 29.86% compared to 29.37% in 2000. However, the moderately high-risk category saw a substantial decrease to 11.45% from 20.98%, and high-risk block groups dropped to 1.08% from 4.05%.

In 2020 (Figure 4.9 C and Table 4.4), the percentage of block groups in the upper Coosa region, categorized as low risk increased markedly to 30.36% from 14.57% in 2010 and 1.37% in 2000. Moderately low risk block groups slightly decreased to 32.48% from 35.90% in 2010 but remained significantly higher than the 12.61% in 2000. Moderate risk block groups decreased to 26.29% from 30.52% in 2010 and 37.66% in 2000. The moderately high-risk category saw a decrease to 10.62% from 18.27% in 2010 and 42.64% in 2000, while high risk dropped to a negligible 0.26% from 0.74% in 2010 and 5.72% in 2000.

The middle Coosa region, including areas such as Cherokee and Etowah counties, also showed progress. The percentage of block groups categorized as low risk increased to 14.54% from 6.13% in 2010 and 5.80% in 2000. Moderately low risk block groups rose to 22.36% from 20.47% in 2010 but decreased from 24.62% in 2000. Moderate risk block groups remained relatively stable at 44.69%, slightly down from 45.97% in 2010 but up from 35.62% in 2000. The moderately high-risk category decreased to 16.81% from 24.92% in 2010 and 26.46% in 2000, while high risk dropped to 1.61% from 2.50% in 2010 and 7.50% in 2000.

The lower Coosa region, including areas such as Shelby and Talladega counties, demonstrated mixed results. The percentage of block groups categorized as low risk decreased to 11.55% from 21.05% in 2010 but remained below 15.59% in 2000. Moderately low risk block groups decreased to 46.21% from 48.93% in 2010 and 61.50% in 2000. Moderate risk block groups increased to 33.44% from 24.43% in 2010 and 15.58% in 2000. The moderately high-risk category decreased to 8.80% from 5.05% in 2010 and 5.89% in 2000, while no block groups were categorized as high risk, down from 0.53% in 2010 and 1.44% in 2000.

For the entire Coosa River watershed in 2020, 24.39% of the block groups were categorized as low risk, a significant increase from 17.98% in 2010 and 12.42% in 2000. The moderately low risk category comprised 33.66% of the watershed, slightly down from 39.63% in 2010 but up from 33.18% in 2000. The proportion of moderate risk block groups increased to 31.30% from 29.86% in 2010 and 29.37% in 2000. The moderately high-risk category saw a decrease to 10.07% from 11.45% in 2010 and 20.98% in 2000, while high risk block groups significantly dropped to 0.57% from 1.08% in 2010 and 4.05% in 2000.

4.4 Bivariate Local Moran's I analysis for social vulnerability & likelihood of contamination associated with flood risk in Coosa River watershed

Similar to the analysis of social vulnerability and the likelihood of contamination associated with flood risk over time, the examination of bivariate cluster categories for social vulnerability and contaminated flood risk throughout the study period reveals trends and shifts in the spatial distribution of these clusters:

Not Significant: No interaction between social vulnerability and contaminated flood risk

High – High Cluster (HH): High social vulnerability and likelihood of contamination associated with flood risk

Low – Low Cluster (LL): Low social vulnerability and low likelihood of contamination associated with flood risk

Low – High Cluster (LH): Low social vulnerability and high likelihood of contamination associated with flood risk

High – Low Cluster (HL): High social vulnerability and low likelihood of contamination associated with flood risk

The study focuses on identifying areas with HH clusters, as these regions are characterized by high socio-economic vulnerability and elevated flood risk.

4.4.1 Scenario for the year 2000:

Figure 4.10 A and Table 4.5 depict that in the upper Coosa region, which includes areas like Rome and Cherokee counties, the percentage of High-High (HH) clusters, indicating areas with both high social vulnerability and high likelihood of contamination associated with flood risk, was significantly high at 25.27%. In contrast, there were no Low-Low (LL) clusters, which denote areas with low social vulnerability and low likelihood of contamination associated with flood risk, suggesting widespread vulnerability in this area. The Low-High (LH) clusters, representing low social vulnerability but high likelihood of contamination associated with flood risk, accounted for 3.69%, while High-Low (HL) clusters, indicating high social vulnerability but low likelihood of contamination associated with flood risk, comprised 11.19%. A significant portion, 59.85%, of the upper Coosa region was not significant, indicating areas without a combination of high or low social vulnerability and flood risk.

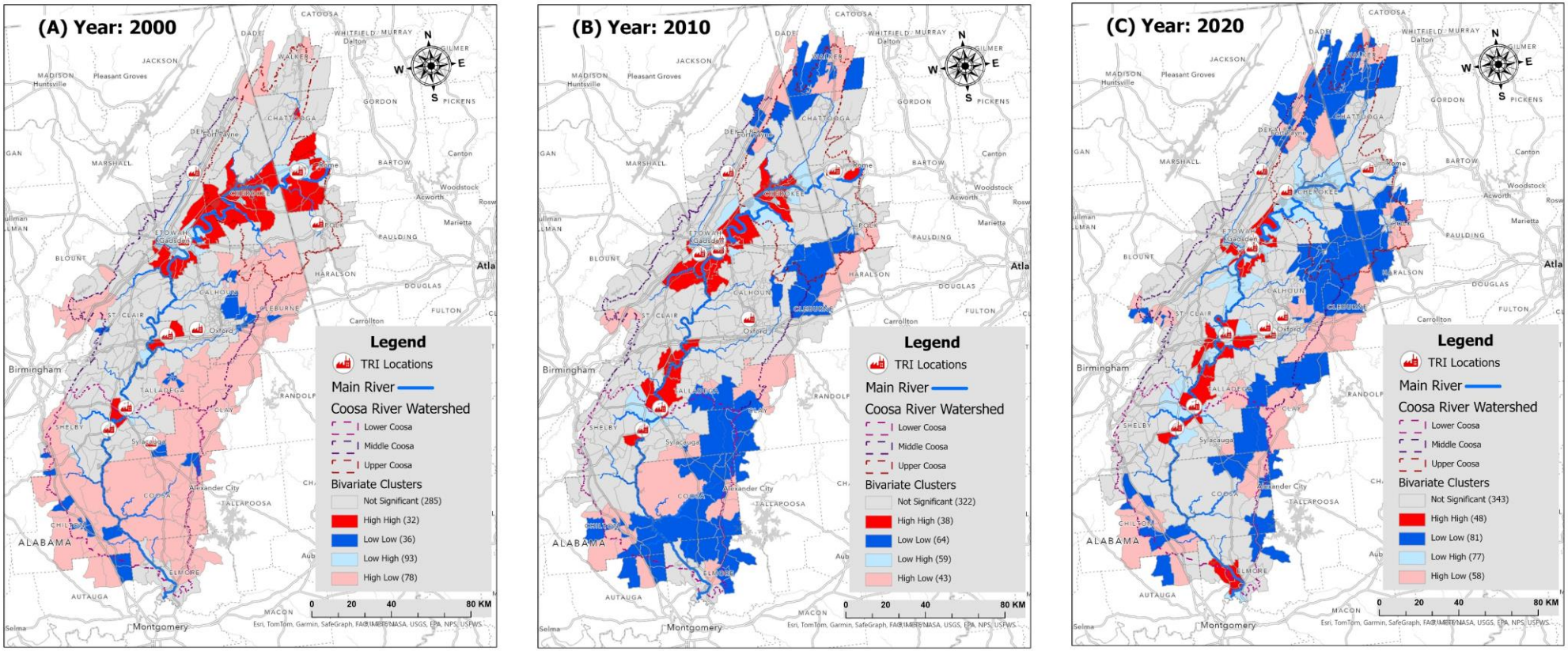

Figure 4.10: Bivariate Local Moran's I cluster map of social vulnerability and likelihood of contamination associated with flood risk in Coosa River watershed for the years 2000, 2010 and 2020.

Table 4.5: Percentage of area of bivariate cluster category for social vulnerability and likelihood of contamination associated with flood risk in different years (for 2000, 2010 and 2020)

Year	River Segment	HH (%)	LL (%)	LH (%)	HL (%)	Not Significant (%)
2000	Upper Coosa	25.27	0	3.69	11.19	59.85
	Middle Coosa	8.95	3.29	4.03	19.97	63.76
	Lower Coosa	1.33	5.35	0.30	65.53	27.49
	Total Coosa watershed	8.62	3.03	2.23	36.73	49.39
2010	Upper Coosa	7.23	18.74	6.5	9.98	57.56
	Middle Coosa	16.04	7.36	3.96	4.7	67.94
	Lower Coosa	0.99	35.36	3.12	21.27	39.26
	Total Coosa watershed	6.82	21.25	3.32	14.84	53.78
2020	Upper Coosa	0	39.82	10.65	10.73	38.8
	Middle Coosa	11.69	12.02	10.69	7.91	57.69
	Lower Coosa	3.42	15.42	4.5	12.25	64.41
	Total Coosa watershed	4.85	22.93	6.8	14.55	50.87

Table 4.6: Major Socio-economic parameters of bivariate cluster categories in different years (for 2000, 2010 and 2020)

Year	Parameters	HH	LL	LH	HL	Not Significant
2000	Total Population (%)	10.35	5.26	10.64	18.8	54.95
	Total Minority (%)	9.31	8.08	16.6	14.46	51.54
	Per capita income (Average)	17467.59	15636.0	15194.23	16578.21	16972.24
	Income less than poverty line (%)	9.17	6.12	14.25	15.46	54.99
2010	Total Population (%)	9.37	8.63	7.15	10.34	64.51
	Total Minority (%)	6.22	8.29	12.63	6.91	65.95
	Per capita income (Average)	25124.05	21124.16	18132.56	20522.23	20808.12
	Income less than poverty line (%)	6.71	7.9	11.34	8.39	65.67
2020	Total Population (%)	10.3	10.53	8.5	12.45	58.22
	Total Minority (%)	12.95	5.12	8.46	10.27	63.2
	Per capita income (Average)	31791.96	27664.12	28387.84	27756.66	30023.58
	Income less than poverty line (%)	10.16	10.42	8.96	11.55	58.91

The middle Coosa region, encompassing parts of Etowah and northwest portion of Talladega counties, exhibited a more diverse distribution of clusters. High-High (HH) clusters covered 8.95% of the area, while Low-Low (LL) clusters accounted for 3.29%. Low-High (LH) clusters made up 4.03%, and High-Low (HL) clusters were significantly high at 19.97%, reflecting a mix of social vulnerability and likelihood of contamination associated with flood risk levels across the region. The remaining 63.76% of the middle Coosa region was not significant, indicating a varied but not overwhelmingly high-risk profile.

In the lower Coosa region, including areas such as Shelby, High-High (HH) clusters were minimal, covering only 1.33% of the area. Low-Low (LL) clusters were more prevalent, accounting for 5.35%, suggesting some areas with lower vulnerability and risk. Low-High (LH) clusters were nearly negligible at 0.30%, while High-Low (HL) clusters dominated at 65.53%, indicating socio-economic challenges despite lower likelihood of contamination associated with flood risk. Not significant areas comprised 27.49% of the lower Coosa region, reflecting a mix of risk and vulnerability profiles.

For the entire Coosa River watershed in 2000, High-High (HH) clusters covered 8.62% of the area. Low-Low (LL) clusters accounted for 3.03%, indicating some areas with minimal risk and vulnerability. Low-High (LH) clusters made up 2.23%, while High-Low (HL) clusters comprised 36.73% of the area. The remaining 49.39% of the watershed was not significant.

The important socio-economic parameters detailed in Table 4.6 further elucidate these findings. High-High (HH) clusters had a total population percentage of 10.35%, with 9.31% of the total minority population living in these areas. The average per capita income in HH clusters was $17,467.59, with 9.17% of the total population living below the poverty line. Low-Low (LL) clusters, representing more stable areas, had a total population percentage of 5.26% and 8.08% of the total minority population. The average per capita income in Low-Low (LL) clusters was $15,636.00, with 6.12% of the total population living below the poverty line. These socio-economic indicators highlight the disparities between different cluster types, emphasizing the need for targeted policy and intervention strategies to address the compounded vulnerabilities in High-High (HH) areas.

4.4.2 Scenario for the year 2010:

Figure 4.10 B and Table 4.5 show that in the upper Coosa region, which includes areas like Rome and Cherokee counties, the percentage of High-High (HH) clusters decreased significantly to 7.23% from 25.27% in 2000. Low-Low (LL) clusters, which denote areas with low social vulnerability and low likelihood of contamination associated with flood risk, emerged to cover 18.74% of the area, compared to none in 2000. Low-High (LH) clusters, representing low social vulnerability but high likelihood of contamination associated with flood risk, increased to 6.5% from 3.69% in 2000, while High-Low (HL) clusters decreased to 9.98% from 11.19% in 2000. The percentage of not significant areas rose to 57.56%, indicating a shift towards more stable conditions.

The middle Coosa region, mostly encompassing parts of Etowah and Talladega counties, exhibited a slight increase in High-High (HH) clusters, which covered 16.04% of the area, up from 8.95% in 2000. Low-Low (LL) clusters also increased to 7.36% from 3.29% in 2000. Low-High (LH) clusters decreased slightly to 3.96% from 4.03% in 2000, while High-Low (HL) clusters decreased significantly to 4.7% from 19.97% in 2000. The remaining 67.94% of the middle Coosa region was not significant, showing a trend towards reduced risk and vulnerability.

In the lower Coosa region, including areas such as Shelby and Elmore counties, High-High (HH) clusters decreased to 0.99% from 1.33% in 2000. Low-Low (LL) clusters increased to 35.36% from 5.35% in 2000. Low-High (LH) clusters slightly increased to 3.12% from 0.30% in 2000, while High-Low (HL) clusters decreased to 21.27% from 65.53% in 2000. Not significant areas increased to 39.26%, reflecting more stable conditions.

For the entire Coosa River watershed in 2010, High-High (HH) clusters covered 6.82% of the area, a decrease from 8.62% in 2000. Low-Low (LL) clusters increased significantly to 21.25% from 3.03% in 2000. Low-High (LH) clusters made up 3.32%, up slightly from 2.23% in 2000, while High-Low (HL) clusters decreased to 14.84% from 36.73% in 2000. The remaining 53.78% of the watershed was not significant, indicating areas without a notable combination of high or low vulnerability and risk.

The major socio-economic parameters detailed in Table 4.6 reveal that High-High (HH) clusters in 2010 had a total population percentage of 9.37%, with 6.22% of the total minority population living in these areas. The average per capita income in HH clusters increased to

$25,124.05, with 6.71% of the population living below the poverty line. Low-Low (LL) clusters, representing more stable areas, had a total population percentage of 8.63% and 8.29% of the total minority population. The average per capita income in LL clusters was $21,124.16, with 7.9% of the population living below the poverty line.

4.4.3 Scenario for the year 2020:

Figure 4.10 C and Table 4.5 exhibit that in the upper Coosa region, the percentage of High-High (HH) clusters decreased to 0% from 7.23% in 2010 and 25.27% in 2000. Low-Low (LL) clusters increased dramatically to 39.82% from 18.74% in 2010 and 0% in 2000, indicating a trend towards stability and reduced risk. Low-High (LH) clusters increased to 10.65% from 6.5% in 2010 and 3.69% in 2000, while High-Low (HL) clusters slightly increased to 10.73% from 9.98% in 2010 but decreased from 11.19% in 2000. The percentage of not significant areas decreased to 38.8%, indicating fewer areas without notable risk and vulnerability.

The middle Coosa region, encompassing parts of Etowah, Calhoun, and Talladega counties, showed a decrease in High-High (HH) clusters to 11.69% from 16.04% in 2010 but remained higher than 8.95% in 2000. Low-Low (LL) clusters decreased to 12.02% from 7.36% in 2010 but remained higher than 3.29% in 2000. Low-High (LH) clusters increased to 10.69% from 3.96% in 2010 and 4.03% in 2000, indicating areas with low social vulnerability but high flood risk. High-Low (HL) clusters decreased to 7.91% from 4.7% in 2010 and 19.97% in 2000. The remaining 57.69% of the middle Coosa region was not significant, indicating a mix of conditions.

In the lower Coosa region, including areas such as Shelby and Elmore counties, High-High (HH) clusters increased to 3.42% from 0.99% in 2010 but remained higher than 1.33% in 2000. Low-Low (LL) clusters decreased significantly to 15.42% from 35.36% in 2010 but were still higher than 5.35% in 2000. Low-High (LH) clusters increased to 4.5% from 3.12% in 2010 and 0.30% in 2000, indicating areas with low social vulnerability but high flood risk. High-Low (HL) clusters decreased to 12.25% from 21.27% in 2010 and 65.53% in 2000. Not significant areas increased to 64.41%, reflecting a trend towards stability and reduced risk.

For the entire Coosa River watershed in 2020, High-High (HH) clusters covered 4.85% of the area, a decrease from 6.82% in 2010 and 8.62% in 2000. Low-Low (LL) clusters increased to 22.93% from 21.25% in 2010 and 3.03% in 2000. Low-High (LH) clusters made up 6.8%, a significant increase from 3.32% in 2010 and 2.23% in 2000, while High-Low (HL) clusters

decreased to 14.55% from 14.84% in 2010 and 36.73% in 2000. The remaining 50.87% of the watershed was not significant, indicating areas without a notable combination of high or low social vulnerability and likelihood of contamination associated with flood risk.

According to Table 4.6, High-High (HH) clusters in 2020 had a total population percentage of 10.3%, with 12.95% of the total minority population living in these areas. The average per capita income in HH clusters increased to $31,791.96, with 10.16% of the population living below the poverty line. Low-Low (LL) clusters, representing more stable areas, had a total population percentage of 10.53% and 5.12% of the total minority population. The average per capita income in LL clusters was $27,664.12, with 10.42% of the population living below the poverty line.

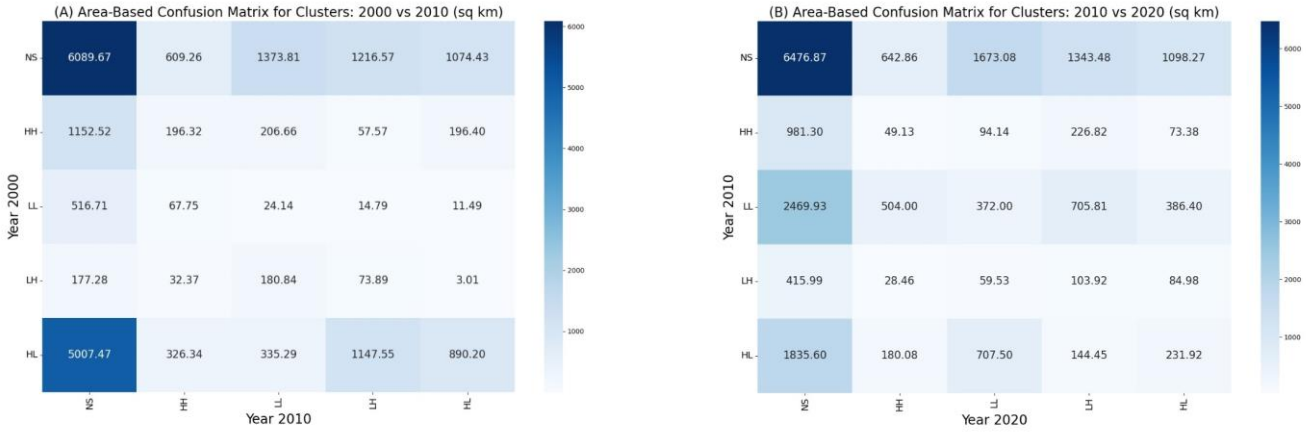

Figure 4.11: Confusion matrices showing changing areas for bivariate clusters of social vulnerability & likelihood of contamination associated with flood risk (2000 vs. 2010 and 2010 vs. 2020)

Confusion matrices offer an additional perspective on the stability and development of at-risk regions over time. Based on the confusion matrices in Figure 4.11 we can see that the trends in bivariate clusters for social vulnerability and contaminated flood risk between 2000, 2010, and 2020 shift. In the 2000 vs 2010 matrix (Figure 4.11 A), the rows represent the cluster categories for the year 2000, while the columns represent the cluster categories for the year 2010. Similarly, in the 2010 vs 2020 matrix (Figure 4.10 B), the rows represent the cluster categories for the year 2010, while the columns represent the cluster categories for the year 2020. Each cell in these matrices indicates the number of areas that have either transitioned from one category in the initial year to another in the subsequent year (off-diagonal cells). Alternatively diagonal cells, where the row and column categories are the same, show the number of areas that have retained their cluster category over the decade, indicating stability in social vulnerability and flood risk interactions.

From 2000 to 2010 (Figure 4.11 A), significant transitions were observed among the High-High (HH) clusters. Of the areas classified as HH in 2000, 1,152.52 sq km remained HH in 2010. However, several areas transitioned to other clusters: 609.26 sq km became Not Significant (NS), 196.32 sq km transitioned to High-Low (HL), and 206.66 sq km to Low-High (LH). These transitions indicate dynamic changes in social vulnerability or flood risk. Conversely, some areas shifted into the HH category from other clusters: 24.14 sq km from Low-Low (LL), 609.26 sq km from NS, and 326.34 sq km from HL. This suggests that certain regions experienced changes, either in increasing social vulnerability or heightened flood risk, resulting in the fluctuation of HH areas. The Low-Low (LL) clusters exhibited notable transitions as well. While 67.75 sq km remained LL, 516.71 sq km shifted to NS, 24.14 sq km to HH, and 14.79 sq km to LH. Similarly, the Low-High (LH) clusters demonstrated significant movement, with 180.84 sq km remaining LH. Key transitions included 32.37 sq km moving to NS, 73.89 sq km to HL, and 3.01 sq km to LL. For the High-Low (HL) clusters, 326.34 sq km remained stable as HL. However, there were notable transitions: 5007.47 sq km shifted to NS, 335.29 sq km to LL, and 1147.55 sq km to LH.

In the 2010 vs 2020 matrix (Figure 4.11 B), the HH clusters continued to show significant transitions. Of the areas classified as HH in 2010, 981.30 sq km remained HH in 2020. However, 49.13 sq km transitioned to NS, 226.82 sq km to HL, and 94.14 sq km to LH, reflecting ongoing dynamic changes. Conversely, shifts into HH from other categories include 372.00 sq km from NS, 707.50 sq km from LH, and 180.08 sq km from HL. The LL clusters exhibited considerable transitions as well. While 504.00 sq km remained LL, 2469.93 sq km shifted to NS, 372.00 sq km to HH, and 705.81 sq km to LH, indicating significant changes in social vulnerability and flood risk. The LH clusters showed considerable movement, with 59.53 sq km remaining LH. Significant transitions included 28.46 sq km moving to NS, 103.92 sq km to HL, and 84.98 sq km to LL. For the HL clusters, 707.50 sq km remained stable as HL. Notable transitions included 1835.60 sq km shifting to NS, 180.08 sq km to LL, and 144.45 sq km to LH, indicating ongoing changes in either social vulnerability or likelihood of contamination with flood risk.

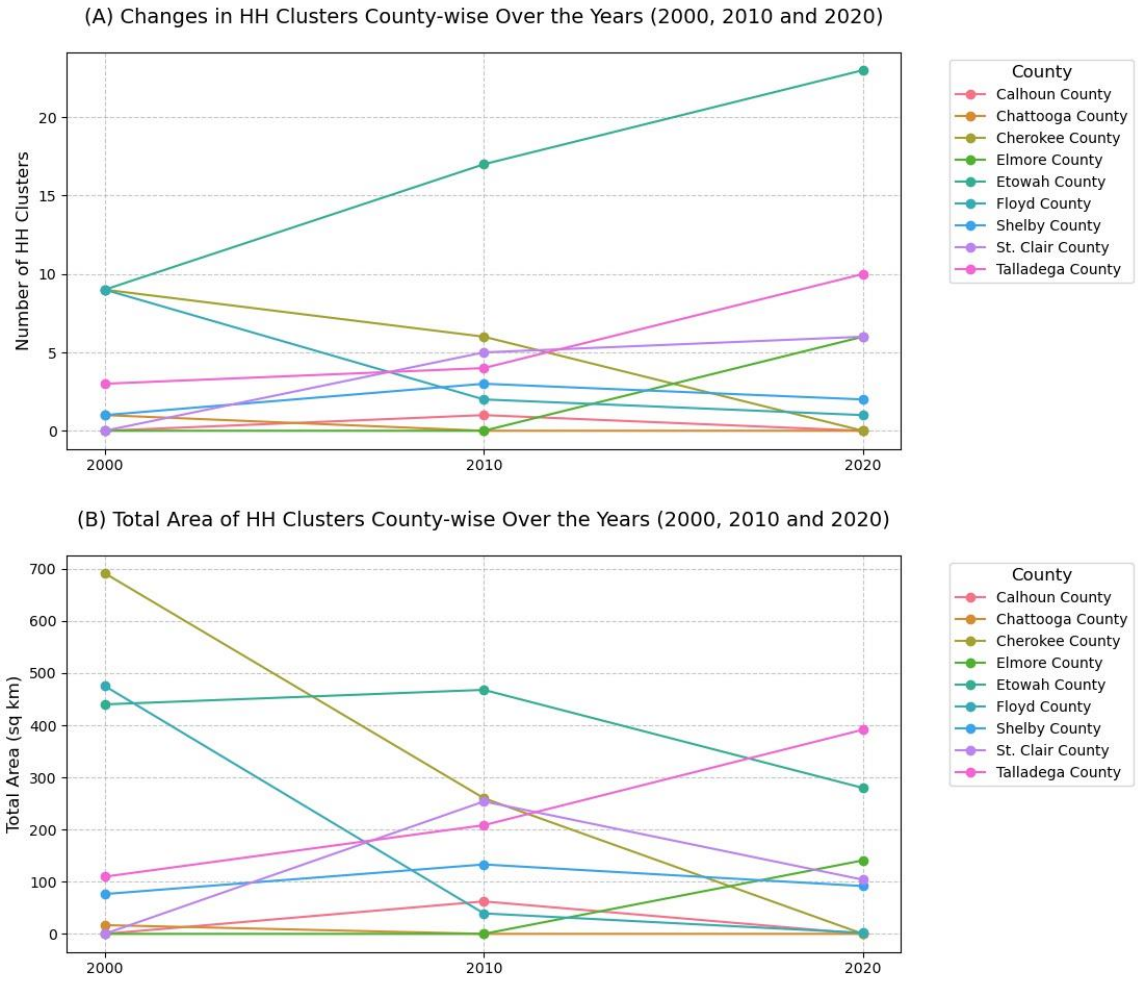

Figure 4.12: Changes in the number and total area of High-High (HH) clusters in various counties within the Coosa River watershed for the years 2000, 2010, and 2020.

Figure 4.12 reveals the changes observed in the number of HH clusters and their total area over the years 2000, 2010, and 2020 across the block groups of various counties that falls within the Coosa River watershed, including Calhoun, Chattooga, Cherokee, Elmore, Etowah, Floyd, Shelby, St. Clair, and Talladega. The first graph (Figure 4.12 A) illustrates the changes in the number of HH clusters over the specified years. Especially, Etowah County exhibits an increase in the number of HH clusters, rising from approximately 9 in 2000 to 21 in 2020. In contrast, counties such as Floyd and Calhoun show a decrease in the number of HH clusters over the same period. Other counties, such as Talladega and Cherokee, display fluctuating trends. The second graph (Figure 4.12 B) depicts the total area covered by the block group of HH clusters across the

counties. A major observation is the reduction in the total area of HH clusters in Elmore County, from approximately 700 square kilometers in 2000 to around 100 square kilometers in 2020. Conversely, counties like Shelby and Talladega exhibit an increase in the total area of HH clusters. It is important to note that, even though some counties, such as Etowah, have an increasing number of HH clusters, the total area of these clusters has been decreasing. This can be attributed to the varying sizes of the block groups within the counties. Smaller block groups may be more numerous but collectively cover less area, whereas fewer larger block groups can cover a more extensive area.

5. Discussion

This research developed a compound hazard assessment approach to analyze the spatial and temporal variations in the intersections of floodwaters, potentially carrying pollutants, with vulnerable communities. The findings highlight significant shifts over time in both the location and extent of pollution, as well as the areas with high and low flood potential. By integrating this information with data on community vulnerability within the study area, a dynamic risk landscape emerges, which varies across different periods and locations. Notably, communities vulnerable to contaminated floodwaters in one period may not be the same in subsequent periods. With this understanding, one of the key takeaways of this work is the need for continually updating information on where vulnerable communities are located and how changes in pollutant discharge interact with flood potential. Several additional findings from this study warrant further consideration.

5.1 Spatial and temporal dynamics of TRI facility discharges in the Coosa River watershed (2000-2020)

A major focus of this study is to understand the dynamics of TRI facilities installations and their chemical discharges to water which informs identification of the likelihood of contamination in flood risk areas. Shifts in location, quantity, and types of chemicals highly impact where these areas are located. Analyzing the total quantity of toxic chemicals released on-site to air, water, and land from these facilities between 2000 and 2020 reveals important trends.

From 2000 to 2020, on-site chemical discharges to surface water showed a stable yet gradually increasing trend, starting at about 0.33 million pounds in 2000 and peaking at 2.02 million pounds in 2020. In contrast, total on-site discharges to air, water, and land significantly

decreased from 19.99 million pounds in 2000 to 6.29 million pounds in 2020, indicating a large reduction in overall toxic emissions to air and land despite an increase in water discharges. The percentage change in these discharges at two-year intervals highlights significant volatility, especially in water discharge changes, which saw a dramatic 575.87% surge in 2004. The total on-site discharge of toxic chemicals, however, showed less severe fluctuations, with a peak increase of 19.28% in 2006 and a significant decrease of 34.26% in 2016, indicating a more consistent reduction trajectory.

The analysis of the top 15 chemicals released to water in 2000, 2010, and 2020 reveals significant shifts in both magnitude and composition. Nitrate Compounds consistently represented the highest quantity of emissions, increasing substantially over time. Zinc Compounds also showed an upward trend, while Barium Compounds and Ammonia decreased. The emergence of new chemicals like Nonylphenol Ethoxylates and Diethanolamine in recent years highlights the evolving nature of chemical discharges. Examining the industry sectors responsible for these emissions highlights varied sources. The distribution of TRI facilities within the Coosa River watershed from 2000 to 2020 shows fluctuations in the number of facilities releasing significant quantities of chemicals. The number of facilities discharging chemicals to surface water varied, peaking at 41 in 2010 and stabilizing at 33 by 2020. The percentage of total TRI facilities releasing chemicals to surface water remained relatively stable, suggesting a consistent proportion of facilities involved in these discharges.

The Emerging Hotspot Analysis map for the Coosa River watershed from 2000 to 2020 visualizes the spatial and temporal dynamics of TRI facilities' discharges. Consecutive hotspots, covering 3.27% of the area, are predominantly in the upper and middle sections of the watershed, particularly around Gadsden. Diminishing cold spots and new hot spots, although smaller, indicate regions with decreasing and emerging discharge levels, respectively. Sporadic hotspots near Gadsden and stable areas in the lower Coosa region show no significant changes in TRI discharge density. In the middle Coosa region around Oxford, the analysis reveals oscillating and persistent cold spots, indicating regions with fluctuating and consistently low discharge levels.

5.2 Social vulnerability to contaminated flood water

Analyzing the Social Vulnerability for communities within the Coosa River watershed from 2000 to 2020 reveals how changing socio-economic conditions have influenced their

vulnerability to flooding and contamination. Over these two decades, the region has seen significant shifts in social vulnerability, reflecting the complex nature of its socio-economic landscape. In the upper Coosa region, including areas like Rome, there was a change from predominantly low to moderately low social vulnerability in 2000 to a more substantial presence of moderately low vulnerability by 2010. This indicated some socio-economic improvements. By 2020, this area experienced a positive shift with an increase in block groups classified as low vulnerability, showing overall socio-economic progress. Meanwhile, the middle Coosa region, covering places such as Gadsden and Oxford, initially showed higher social vulnerability in 2000, with many block groups marked as moderate to moderately high vulnerability. This trend continued into 2010, suggesting ongoing socio-economic challenges. However, by 2020, the middle Coosa region saw improvements, with more block groups falling into the low vulnerability category and fewer in the moderate range, indicating a reduction in socio-economic pressures. The lower Coosa region, including areas like Sylacauga and Talladega, had a varied social vulnerability profile in 2000, with a notable portion of block groups in the high vulnerability category. By 2010, many block groups were in the moderately low and moderate categories, indicating mixed progress. By 2020, this region showed significant improvements, with an increase in low vulnerability block groups and a decrease in moderate vulnerability, reflecting positive socio-economic changes. Overall, the Coosa River watershed experienced a substantial increase in block groups categorized as low vulnerability by 2020, signaling positive socio-economic developments over the two decades. Despite this progress, areas like Etowah, St. Clair, and Calhoun counties continued to face challenges, as shown by the presence of block groups with moderate to moderately high vulnerability. These findings highlight the dynamic nature of social vulnerability within the Coosa River watershed. The trend towards increased social vulnerability in certain areas like Etowah, St. Clair, and Calhoun counties suggests these communities are now at greater risk of the adverse effects of combined hazards, such as floods mixed with chemical contaminants, complicating recovery efforts and resource allocation after natural disasters.

In terms of the likelihood of contamination with flood risk patterns, notable shifts have been revealed within the Coosa River watershed over the past two decades. The Upper Coosa region, encompassing Walker, Rome, DeKalb, and Chattooga counties, initially displayed a high proportion of block groups at moderate to high risk levels. In 2000, over 42% of block groups were classified as moderately high risk, and nearly 6% as high risk. However, by 2020, there was a

marked improvement. The percentage of high-risk areas dropped to nearly negligible levels, with a significant increase in low-risk block groups from 1.37% in 2000 to over 30% in 2020. This positive trend underscores improved environmental conditions in the region. In contrast, the Middle Coosa region, including Cherokee and Etowah counties, showed a more complex pattern. Initially, this area had a mix of moderate and high-risk levels, with 36% of block groups at moderate risk and 7.5% at high risk in 2000. By 2020, there was an increase in low-risk areas, rising to 14.54%, and a reduction in high-risk block groups to 1.61%. However, the proportion of moderate-risk areas remained relatively stable, indicating an environmental risk despite some improvements. The Lower Coosa region, which includes Talladega, Shelby, and Elmore counties, presented a distinct profile. In 2000, this region predominantly featured lower risk levels, with over 61% of block groups classified as moderately low risk. Over the next two decades, the region saw a decrease in low-risk areas but also a reduction in high-risk block groups to zero by 2020. Despite this improvement, the proportion of moderate-risk areas increased, suggesting a shift in vulnerabilities rather than a uniform reduction in risk. In general, the Coosa River watershed experienced a general improvement in contamination risks associated with floods from 2000 to 2020. The Upper Coosa region's gradual decrease in high-risk areas highlights decreasing environmental challenges. In the Middle Coosa region, while some progress was made, the persistence of moderate-risk areas points to ongoing environmental challenges. The Lower Coosa region's reduction in high-risk block groups to zero is notable, although the increase in moderate-risk areas indicates evolving vulnerabilities that require attention.

Combining social vulnerability and contaminated flood risk, the Bivariate LISA analysis over the past two decades has highlighted significant variations across multiple counties in the Coosa River watershed (Tables 4.5 and 4.6). In the upper Coosa region, including Rome and Cherokee counties, the transformation of HH clusters is particularly striking. In 2000, this region faced challenges, with a high portion of the area characterized by HH clusters, indicating a severe combination of social vulnerability and contamination risk. However, by 2020, these high-risk zones had completely disappeared. The middle Coosa region, encompassing parts of Etowah, Calhoun, and Talladega counties, presents a more nuanced picture. Initially, the region saw an increase in HH clusters, reflecting growing areas of concern. By 2010, the percentage of HH clusters had risen, indicating that the region continued to grapple with significant socio-economic and environmental challenges. However, by 2020, there was a noticeable decrease in these high-

risk areas, although they remained more prevalent than in the early 2000s. In the lower Coosa region, including Shelby and Elmore counties, HH clusters have been consistently minimal over the years. In 2000, the presence of these high-risk zones was already low, and while there was a slight increase by 2020, the overall extent remained limited compared to other regions. This pattern indicates that, while some areas have emerged as new concerns, the lower Coosa region has generally maintained a lower level of compounded vulnerability. In general, the entire Coosa River watershed exhibits a trend towards a reduction in HH clusters from 2000 to 2020. The initial high presence of these clusters in 2000 highlighted critical areas requiring urgent intervention. By 2010, some regions saw an increase in HH clusters, underscoring ongoing challenges. However, the significant decrease in HH clusters by 2020 across many areas of the watershed such as Rome, Cherokee, Etowah, Calhoun, Talladega, Shelby, and Elmore counties reflects positive strides in addressing the factors contributing to high social vulnerability and contamination risk.

The observed shifts in High-High (HH) clusters within the Coosa River watershed indicate a multifaceted and dynamic interplay between various environmental and socio-economic factors, each contributing to the evolving risk patterns. Notably, fluctuations in geographic parameters, such as increased rainfall or extreme drought events in a particular year, can significantly impact the spatial distribution of inundation-prone areas. Concurrently, the shifting landscape of Toxic Release Inventory (TRI) facilities, including modifications in their operational scales, locations, and the types of chemicals released, has further influenced these patterns. Additionally, socio-economic changes within the watershed, such as population growth, economic fluctuations, and improvements or declines in infrastructure, have affected social vulnerability indices. These indices reflect the community's capacity to respond to and recover from environmental hazards. The convergence of these factors creates a complex risk environment where no single element can be isolated as the primary driver. Instead, it is the interactive effects of flooding dynamics, industrial activity, and socio-economic conditions that collectively shape the risk landscape. This complexity underscores the importance of using comprehensive and integrative methodological approaches, like the Analytic Hierarchy Process (AHP) employed in this study, to capture the intricate and interdependent nature of these influences.

5.3 Effectiveness of the methodological framework

The selection of variables for creating the Social Vulnerability Index (SoVI) is particularly well-suited for this study, capturing the socio-economic dimensions that contribute to a community's susceptibility to contaminated floodwaters. Variables such as higher minority populations often correlate with limited resource access and increased exposure to environmental hazards. Low educational attainment can hinder disaster preparedness and recovery, while income levels influence a household's capacity to respond effectively to floods. The presence of children and elderly individuals increases vulnerability due to their need for assistance during disasters. This comprehensive approach ensures that the SoVI effectively reflects the underlying vulnerabilities within the community.

Analyzing temporal changes in the SoVI from 2000, 2010, and 2020 indicates that some communities consistently exhibit vulnerability across all periods, while others do so intermittently. For instance, vulnerability remained moderate to high across all three years (2000, 2010, and 2020) in the parts of the Middle and Lower Coosa regions, particularly around Etowah, St. Clair, and Talladega counties. These regions consistently showed significant proportions of block groups classified as moderate to moderately high vulnerability, highlighting persistent socio-economic challenges. On the other hand, vulnerability improved primarily in the Upper Coosa region, including parts of Rome and surrounding areas. These regions showed an increasing in low vulnerability categories and a decrease in moderate to high vulnerability over the two decades, indicating notable socio-economic improvements. This dynamic nature of social vulnerability underscores the need for regular reassessment to ensure that the most vulnerable populations can access necessary information and resources.

The methodology’s integration of multiple risk factors using the Analytic Hierarchy Process (AHP) significantly enhances the comprehensiveness and effectiveness of the flood risk and contaminant exposure analysis. By combining diverse data inputs (as outlined in Table 3.2), the framework ensures a robust assessment that accounts for critical variables influencing flood and contamination risks. The sensitivity of the methodology to various data inputs, such as precipitation and TRI density, demonstrates its adaptability to evolving environmental and socio-economic conditions. This sensitivity analysis highlights the importance of regularly updating and validating data inputs to maintain the accuracy and relevance of the risk assessment.

5.4 Significance of the study

The significance of this study lies in its new approach to integrating multiple dynamic factors including TRI data to assess environmental risk, distinguishing it from prior research in the field. Unlike earlier studies, such as those by Cutter et al. (2003) and Boruff et al. (2005), which primarily focused on social vulnerability and physical parameters respectively, this research uniquely incorporates Toxic Release Inventory (TRI) data, a critical yet previously neglected component in contaminated flooding studies. Cutter et al. (2003) introduced the Social Vulnerability Index (SoVI), which measures the influence of socio-economic and demographic factors on community resilience to environmental hazards. Boruff et al. (2005) expanded this work by examining coastal vulnerability, blending physical and social factors to understand variations in vulnerability. However, neither study accounted for the role of industrial activities and the release of toxic chemicals, which are essential for comprehending contaminated flood risks. The integration of TRI data in this study, including the location, quantity, and types of chemicals released by industrial facilities, represents a unique approach that provides a more comprehensive environmental risk assessment.

The ability to track shifts in High-High (HH) clusters areas with high social vulnerability and high environmental risk over time reveals how dynamic interactions between flooding, industrial activities, and socio-economic conditions influence risk patterns. The findings indicate that these cluster movements are not attributed to a single factor but rather the combined effects of changing flood dynamics, TRI facility operations, and socio-economic conditions. This integrative approach provides a holistic view of evolving risks, offering valuable insights for developing adaptive and effective risk management strategies.

This research also aligns with similar works, such as those by Chakraborty et al. (2014) and Rufat et al. (2019), which emphasized the need for vulnerability assessments that include both social and environmental factors. However, by incorporating TRI data, this study fills a critical gap in previous research, providing a more detailed understanding of contaminated flood risks. This advancement has implications for policy and management, underscoring the necessity for regulations that address both environmental hazards and industrial activities to protect vulnerable communities effectively.

6. Limitations and future research directions

The study encountered several limitations that are crucial to acknowledge for future research endeavors. The temporal scope of this analysis was confined to three specific years: 2000, 2010, and 2020. While this timeframe provides valuable insights into temporal changes, it may not fully capture the dynamic aspects of social vulnerability and environmental conditions over shorter periods. Additionally, the application of the Analytic Hierarchy Process (AHP) introduces limitations due to its reliance on subjective judgment in assigning weights to various risk factors. Despite validating these weights through the Consistency Ratio (CR), they may not accurately represent the real-world significance of each factor (Saaty, 2008; Ishizaka & Labib, 2011). Furthermore, this research considered only 11 socio-economic and 11 environmental and pollution parameters, which could affect the outcome. Expanding the number of parameters could alter the results, as the current findings only reflect the provided parameters (Malczewski, 2006; Rezaei, 2015). There are also uncertainties in the results when identifying areas likely to experience contamination associated with flood risk, as the methodology cannot precisely determine the amount or types of chemicals that might be dispersed in those locations. It only indicates a high probability of areas where such contaminations might occur (Jonkman et al., 2008; Merz et al., 2010).

Moreover, in Bivariate Local Moran's I analysis, the degree of correlation between areas of social vulnerability and the likelihood of contaminations associated with flood risk variables at a local level suggests that high or low values of one variable are often associated with corresponding high or low values of another variable. While the results indicate that a higher proportion of people are at risk and a higher proportion of areas are likely to experience contaminations associated with flood risk, this does not necessarily imply that all individuals in these areas are vulnerable or that all regions have a high likelihood of contamination. The methodology may not adequately account for spatial heterogeneity, where different processes might be at work in various parts of the study area, potentially leading to misleading conclusions if the local context is not carefully considered (Ge et al., 2017; Cutter et al., 2003). Spatial heterogeneity can significantly influence risk assessments, and without accounting for local variations, the analysis may overlook critical factors influencing vulnerability and risk (Schmidtlein et al., 2008; Tate, 2012).

The study analyzed datasets from 2000, 2010, and 2020, using PRISM High-Resolution Spatial Climate Data for annual average precipitation due to its availability from 2000 onwards and its superior spatial resolution of about 4 km (PRISM Climate Group, 2024) compared to other precipitation datasets. This data had to be resampled to match the 30 m resolution of other raster datasets used in the study, such as Digital Elevation Model (DEM), slope, distance from the main river, distance from Toxic Release Inventory (TRI) sites, Topographic Wetness Index (TWI), Land Use/Land Cover (LULC) map, drainage density, and TRI density. Resampling was necessary because some block groups are smaller than 4 square km, and without it, the finer-scale details of these groups couldn't be captured accurately (Chowdhury et al., 2019; Yu et al., 2013). Although the resampling process might seem weighty, it's important to note that precipitation data contributed only 14% to the total weights in the Analytical Hierarchy Process (AHP) technique, while the other 10 parameters made up 86%. This means that the resampling had a minimal impact on the overall spatial analysis of the block groups (Wang et al., 2018; Zhang et al., 2021). Resampling precipitation data is a common practice in environmental studies to maintain consistency and accuracy, and this study followed that same approach to ensure precise results (Johnson & Johnson, 2015; Smith et al., 2017).

In this study, the analysis units are the block groups within the Coosa River watershed for the years 2000, 2010, and 2020. Over these decades, a few of the block groups have experienced changes. For each specific time period, the relevant block groups were analyzed, meaning the results displayed in the maps for 2000, 2010, and 2020 represent the block groups' areas pertinent to each respective time frame. When generating the confusion matrix of the Bivariate Local Moran's I result, the analysis focuses on the percentage of the area covered by these clusters is considered, ensuring that the unique characteristics and changes in block groups over time are accounted for. Additionally, while running the Emerging Hotspot Analysis, block groups from 2020 were utilized to extract data as a space-time bin to maintain consistency across the years.

To address the limitations identified in this study and enhance future research, several avenues can be explored. Improving data collection methods is crucial for ensuring more accurate, up-to-date, and comprehensive datasets. Leveraging advanced remote sensing technologies and crowd-sourced data can fill existing gaps, particularly in capturing real-time information. Expanding the temporal scope of the study to include more frequent intervals can offer further

understanding of the dynamics of social vulnerability and flood risk, revealing short-term changes and trends that might be overlooked in decadal analyses.

Future research should also consider incorporating additional socio-economic and environmental variables that influence vulnerability and risk. Including factors such as healthcare access, percentage of people with disabilities, social capital, community resilience etc. could provide a more holistic perspective on vulnerability. Enhancing methodologies for risk assessment by exploring alternative multi-criteria decision analysis techniques or integrating machine learning algorithms can improve the robustness and accuracy of the results. Moreover, addressing spatial heterogeneity more effectively through localized models that account for different processes in various parts of the study area is essential for avoiding misleading conclusions and ensuring a comprehensive risk assessment.

This study lays the groundwork for identifying areas where socially vulnerable populations may face dual threats: the immediate danger of flooding and the long-term impact of contamination from industrial emissions carried by floodwaters. Mapping regions of high social vulnerability alongside probable areas at risk of contamination due to flooding helps us better understand the compounded risks these communities face. Floodwaters not only pose a physical threat but also carry industrial pollutants, which can have prolonged detrimental effects on health and the environment. Future research should evaluate the effectiveness of policies and interventions aimed at reducing social vulnerability, industrial emissions, and flood risk. Such evaluations can offer valuable feedback for policymakers, aiding in the refinement of strategies for better outcomes.

Engaging local communities in the research process can provide deeper insights into socio-economic realities and enhance the relevance and applicability of the findings. Participatory approaches empower communities and build local capacity for disaster risk management. By addressing these limitations and pursuing these future research directions, it is possible to develop more comprehensive and effective strategies for managing social vulnerability and flood risk in dynamic environmental contexts.

References

Abdel-Satar, A. M., Ali, M. H., & Goher, M. E. (2017). Indices of water quality and metal pollution of Nile River, Egypt. *Egyptian Journal of Aquatic Research, 43*(1), 21–29. https://doi.org/10.1016/j.ejar.2016.12.006

Adikari, Y., & Yoshitani, J. (2009). *Global trends in water-related disasters: An insight for policymakers*. United Nations World Water Assessment Programme.

Abdrabo, K. I., Kantoush, S. A., Esmaiel, A., Saber, M., Sumi, T., Almamari, M., Elboshy, B., & Ghoniem, S. (2023). An integrated indicator-based approach for constructing an urban flood vulnerability index as an urban decision-making tool using the PCA and AHP techniques: A case study of Alexandria, Egypt. *Urban Climate, 48*, 101426. https://doi.org/10.1016/j.uclim.2023.101426

Alabama Department of Environmental Management (ADEM). (2023). *Industrial activity and environmental regulation in Etowah County*. Retrieved from https://www.adem.alabama.gov/industrial-activity-etowah-county

Alabama Department of Environmental Management (ADEM). (2022). *2022 Alabama 303(d) list fact sheet*. Retrieved from https://adem.alabama.gov/programs/water/wquality/2022AL303dFactSheet.pdf

Al-Abadi, A. M., Shahid, S., & Al-Ali, A. K. (2016). A GIS-based integration of catastrophe theory and analytical hierarchy process for mapping flood susceptibility: A case study of Teeb area, southern Iraq. *Environmental Earth Sciences, 75*(7), 687. https://doi.org/10.1007/s12665-016-5523-7

Allison, E., & Cho, V. (2020). River conservation by an Indigenous community. *Nature*, 588, 589 - 590. https://doi.org/10.1038/d41586-020-03316-y.

Alulema-Pullupaxi, P., Espinoza-Montero, P. J., Sigcha-Pallo, C., Vargas, R., Fernández, L., Peralta-Hernández, J. M., & Paz, J. L. (2021). Fundamentals and applications of photoelectrocatalysis as an efficient process to remove pollutants from water: A review. *Chemosphere, 281*, 130821. https://doi.org/10.1016/j.chemosphere.2021.130821

Alfieri, L., Salamon, P., Bianchi, A., Neal, J., Bates, P., & Feyen, L. (2013). Advances in pan-European flood hazard mapping. *Hydrological Processes*. https://doi.org/10.1002/hyp.9947

American Rivers. (2022). Coosa River named among America's most endangered rivers of 2022. American Rivers. https://www.americanrivers.org/media-item/coosa-river-named-among-americas-most-endangered-rivers-of-2022/

Anselin, L. (1995). Local indicators of spatial association—LISA. *Geographical Analysis, 27*(2), 93–115. https://doi.org/10.1111/j.1538-4632.1995.tb00338.x

Anselin, L., Li, X., & Koschinsky, J. (2022). GeoDa, from the desktop to an ecosystem for exploring spatial data. *Geographical Analysis, 54*(3), 439-466. https://doi.org/10.1111/gean.12258

Atoba, K., Newman, G., & Sansom, G. (2023). Multi-hazard property buyouts: Making a case for the acquisition of flood and contaminant-prone residential properties in Galena Park, TX. *Climate Risk Management, 41*, 100529. https://doi.org/10.1016/j.crm.2023.100529

Beven, K. J., & Kirkby, M. J. (1979). A physically based, variable contributing area model of basin hydrology/Un modèle à base physique de zone d'appel variable de l'hydrologie du bassin versant. *Hydrological Sciences Journal, 24*(1), 43–69.

Blaikie, P., Cannon, T., Davis, I., & Wisner, B. (1994). *At risk: Natural hazards, people's vulnerability, and disasters*. London, UK: Routledge.

Boruff, B. J., Emrich, C., & Cutter, S. L. (2005). Erosion hazard vulnerability of US coastal counties. *Journal of Coastal Research, 21*(5), 932-942.

Butter, M. E. (2006). Are women more vulnerable to environmental pollution? *Journal of Human Ecology, 20*(3), 221–226. https://doi.org/10.1080/09709274.2006.11905931

Coosa River Basin Management Plan. (1998). Georgia Department of Natural Resources Environmental Protection Division. Retrieved from https://epd.georgia.gov/document/publication/coosa-river-basin-management-planpdf/download

Conley, J. F. (2011). Estimation of exposure to toxic releases using spatial interaction modeling. *International Journal of Health Geographics, 10*, 20. https://doi.org/10.1186/1476-072X-10-20

Ciszewski, D. (2001). Flood-related changes in heavy metal concentrations within sediments of the Biała Przemsza River. *Geomorphology, 40*(3-4), 205–218. https://doi.org/10.1016/S0169-555X(01)00044-7

Chakraborty, J., Collins, T. W., & Grineski, S. E. (2014). Social vulnerability to environmental hazards. In S. L. Cutter (Ed.), *Social vulnerability to disasters* (pp. 259-280). Springer.

Chowdhury, R., Das, S., & Roy, P. (2019). Impact of resampling on precipitation data. Environmental Modelling & Software, 114, 79-91.

Crawford, S. E., Brinkmann, M., Ouellet, J. D., Lehmkuhl, F., Reicherter, K., Schwarzbauer, J., Bellanova, P., Letmathe, P., Blank, L. M., Weber, R., Brack, W., van Dongen, J. T., Menzel, L., Hecker, M., Schüttrumpf, H., & Hollert, H. (2021). Remobilization of pollutants during extreme flood events poses severe risks to human and environmental health. *Journal of Hazardous Materials, 421*, 126691. https://doi.org/10.1016/j.jhazmat.2021.126691

Chagué-Goff, C., Niedzielski, P., Wong, H. K. Y., Szczuciński, W., Sugawara, D., & Goff, J. (2012). Environmental impact assessment of the 2011 Tohoku-oki tsunami on the Sendai Plain. *Sedimentary Geology, 282*, 175–187. https://doi.org/10.1016/j.sedgeo.2012.06.002

Collins, T. W., Grineski, S. E., & Chakraborty, J. (2018). Environmental injustice and flood risk: A conceptual model and case comparison of metropolitan Miami and Houston, USA. *Regional Environmental Change, 18*(2), 311–323. https://doi.org/10.1007/s10113-017-1121-9

Coosa River at Wetumpka AL. USGS Water Data for the Nation. (n.d.). Retrieved from https://waterdata.usgs.gov/monitoring-location/02411600/#parameterCode=00065&period=P7D

Cutler, D. M., & Miller, G. (2005). The role of public health improvements in health advances: The twentieth-century United States. *Demography, 42*(1), 1-22.

Cutter, S. L., Boruff, B. J., & Shirley, W. L. (2003). Social vulnerability to environmental hazards. *Social Science Quarterly, 84*(2), 242–261. http://www.jstor.org/stable/42955868

Danumah, J. H., Odai, S. N., Saley, B. M., Szarzynski, J., Thiel, M., Kwaku, A., & Kouame, F. K. (2016). Flood risk assessment and mapping in Abidjan district using multi-criteria analysis (AHP) model and geoinformation techniques, (Cote d'Ivoire). *Geoenvironmental Disasters, 3*(1), 10. https://doi.org/10.1186/s40677-016-0044-y

da Rocha, M. L., Sa, F., Campos, M. S., Grassi, M. T., Combi, T., & Machado, E. C. (2017). Metals impact into the Paranaguá estuarine complex (Brazil) during the exceptional flood of 2011. *Brazilian Journal of Oceanography, 65*(1), 54–68. https://doi.org/10.1590/S1679-87592017127706501

de Moel, H., Jongman, B., Kreibich, H., Merz, B., Penning-Rowsell, E., & Ward, P. J. (2015). Flood risk assessments at different spatial scales. *Mitigation and Adaptation Strategies for Global Change, 20*(6), 865–890. https://doi.org/10.1007/s11027-015-9654-z

Dodgson, J. S., Spackman, M., Pearman, A., & Phillips, L. D. (2009). *Multi-criteria analysis: A manual* (Vol. 11). Department for Communities and Local Government Publication. ISBN 9781409810230.

Dragičević, N., Karleuša, B., & Ožanić, N. (2019). Different approaches to estimation of drainage density and their effect on the erosion potential method. *Water, 11*(3), 593. https://doi.org/10.3390/w11030593

Ebenstein, A. (2012). The consequences of industrialization: Evidence from water pollution and digestive cancers in China. *Review of Economics and Statistics, 94*(1), 186-201.

Estis, W. (2008). The impacts of river impoundment: A case study of H. Neely Henry Lake in northeast Alabama [Master of Science, Louisiana State University and Agricultural and Mechanical College]. https://doi.org/10.31390/gradschool_theses.1659

Esri. (2021). *How Hot Spot Analysis (Getis-Ord Gi*) works—Help/ArcGIS Desktop*. Esri. https://pro.arcgis.com/en/pro-app/latest/tool-reference/spatial-statistics/h-how-hot-spot-analysis-getis-ord-gi-spatial-stati.htm

Eubanks, M. (2001). Environmental Analysis for Water Allocation in the ACT and ACF River Basins: Water Quality and Freshwater Resources. https://doi.org/10.1061/40499(2000)149.

Euripidou, E., & Murray, V. (2004). Public health impacts of floods and chemical contamination. *Journal of Public Health (Bangkok), 26*(4), 376–383. https://doi.org/10.1093/pubmed/fdh163

Fadia, F. M., Moradi, H., Massah, A. R. B., Panahi, M., Berndtsson, R., & Hashemi, H. (2019). Climate change impact on flood frequency and source area in Northern Iran under CMIP5 scenarios. *Water, 11*(2), 273. https://doi.org/10.3390/w11020273

Farhadian, M., Bozorg-Haddad, O., Pazoki, M., & Loáiciga, H. A. (2019). Minimal adverse impact of discharging polluted effluents to rivers with selective locations. *Sustainable Cities and Society, 46*, 101394. https://doi.org/10.1016/j.scs.2018.12.022

Fernandez, D., & Lutz, M. (2010). Urban flood hazard zoning in Tucumán Province, Argentina, using GIS and multicriteria decision analysis. *Engineering Geology, 111*(1-4), 90–98.

Fekete, A. (2009). Validation of a social vulnerability index in context to river-floods in Germany. *Natural Hazards and Earth System Sciences, 9*(2), 393–403. https://doi.org/10.5194/nhess-9-393-2009

Förstner, U., Hollert, H., Brinkmann, M., Eichbaum, K., Weber, R., & Salomons, W. (2016). Dioxin in the Elbe river basin: Policy and science under the water framework directive 2000–2015 and toward 2021. *Environmental Sciences Europe, 28*, 9. https://doi.org/10.1186/s12302-016-0075-8

Foulds, S. A., Brewer, P. A., Macklin, M. G., Haresign, W., Betson, R. E., & Rassner, S. M. E. (2014). Flood-related contamination in catchments affected by historical metal mining: An unexpected and emerging hazard of climate change. *Science of the Total Environment, 476–477*, 165–180. https://doi.org/10.1016/j.scitotenv.2013.12.079

Gangrade, S., Kao, S., Naz, B., Rastogi, D., Ashfaq, M., Singh, N., & Preston, B. (2018). Sensitivity of Probable Maximum Flood in a Changing Environment. *Water Resources Research*, 54, 3913 - 3936. https://doi.org/10.1029/2017WR021987.

Gao, J., Zhao, Y., Zhang, A., & Wang, H. (2020). Variations of future extreme floods in the context of climate change. *Water Resources Research*. https://doi.org/10.1029/2019WR026684

Goto, K., Fujima, K., Sugawara, D., Fujino, S., Imai, K., Tsudaka, R., Abe, T., & Haraguchi, T. (2012). Field measurements and numerical modeling for the run-up heights and inundation distances of the 2011 Tohoku-oki tsunami at Sendai Plain, Japan. *Earth, Planets and Space, 64*(11), 1247–1257. https://doi.org/10.5047/eps.2012.02.007

Ge, Y., Dou, W., & Gu, Z. (2017). A spatial analysis of social vulnerability and flood risk in the Zhejiang Province of China. *Sustainability*, 9(4), 613.

Getis, A., & Ord, J. K. (1992). The Analysis of Spatial Association by Use of Distance Statistics. *Geographical Analysis*, *24*(3), 189–206. https://doi.org/10.1111/J.1538-4632.1992.TB00261.X/ABSTRACT

Greene, R., Devillers, R., Luther, J. E., & Eddy, B. G. (2011). GIS-based multiple-criteria decision analysis. *Geography Compass, 5*(6), 412-432.

Guntara, I. (2013). Understanding overlays in geographic information systems. Retrieved from http://www.guntara.com/2013/01/pengertian-overlay-dalam-sistem.html

Halder, J., & Islam, N. (2015). Water pollution and its impact on human health. *Journal of Environment and Human, 2*(1), 36–46. https://doi.org/10.15764/EH.2015.01005

Hassanzadeh, E., Strickert, G., Morales-Marín, L., Noble, B., Baulch, H., Shupena-Soulodre, E., & Lindenschmidt, K. (2019). A framework for engaging stakeholders in water quality modeling and management: Application to the Qu'Appelle River Basin, Canada. *Journal of environmental management*, 231, 1117-1126. https://doi.org/10.1016/j.jenvman.2018.11.016.

Hermans, C., Erickson, J., Noordewier, T., Sheldon, A., & Kline, M. (2007). Collaborative environmental planning in river management: An application of multicriteria decision analysis in the White River watershed in Vermont. *Journal of Environmental Management, 84*(4), 534-546.

Hicks, A., Malone, Z., Moore, M., Powell, R., Thompson, A., Whitener, P., & Williams, R. (2021). Green inequities: Examining the dimensions of socioenvironmental injustice in marginalized communities. *Parks Stewardship Forum*. https://doi.org/10.5070/p537354736.

Hirabayashi, Y., & Kanae, S. (2009). First estimate of the future global population at risk of flooding. *Hydrological Research Letters, 3*, 6–9. https://doi.org/10.3178/hrl.3.6

Horney, J. A., Casillas, G. A., Baker, E., Stone, K. W., Kirsch, K. R., Camargo, K., Wade, T. L., & McDonald, T. J. (2018). Comparing residential contamination in a Houston environmental justice neighborhood before and after Hurricane Harvey. *PLoS One, 13*, e0192660. https://doi.org/10.1371/journal.pone.0192660

Ishizaka, A., & Labib, A. (2011). Review of the main developments in the analytic hierarchy process. *Expert Systems with Applications, 38*(11), 14336-14345.

Iqbal, J., Gisclair, D., McMillin, D. J., & Portier, R. J. (2007). Aspects of petrochemical pollution in southeastern Louisiana (USA): Pre-Katrina background and source characterization. *Environmental Toxicology and Chemistry, 26*(9), 2001–2009. https://doi.org/10.1897/07-077.1

Jalan, J., & Ravallion, M. (2003). Does piped water reduce diarrhea for children in rural India? *Journal of Econometrics, 112*(1), 153-173.

Jenks, G. F. (1967). The data model concept in statistical mapping. *International Yearbook of Cartography, 7*, 186–190.

Jones, K. W., Snyder, N. P., & White, E. M. (2018). *Assessing the temporal stability of topographic parameters derived from DEMs and their implications for hydrological modeling*. Journal of Hydrology, 567, 234-245.

Jongman, B., Ward, P. J., & Aerts, J. C. J. H. (2012). Global exposure to river and coastal flooding—long term trends and changes. *Global Environmental Change, 22*(4), 823–835. https://doi.org/10.1016/j.gloenvcha.2012.07.004

Jonkman, S. N., Bockarjova, M., Kok, M., & Bernardini, P. (2008). Integrated hydrodynamic and economic modelling of flood damage in the Netherlands. *Ecological Economics, 66*(1), 77-90.

Johnson, M. P., & Johnson, S. D. (2015). Spatial resampling of precipitation data for environmental modeling. Environmental Monitoring and Assessment, 187, 348.

Kazakis, N., Kougias, I., & Patsialis, T. (2015). Assessment of flood hazard areas at a regional scale using an index-based approach and analytical hierarchy process: Application in Rhodopee Evros region, Greece. *Science of the Total Environment, 538*, 555–563. https://doi.org/10.1016/j.scitotenv.2015.08.055

König, M., Escher, B., Neale, P., Krauss, M., Hilscherová, K., Novák, J., Teodorović, I., Schulze, T., Seidensticker, S., Hashmi, M. A. K., Ahlheim, J., & Brack, W. (2017). Impact of untreated wastewater on a major European river evaluated with a combination of in vitro bioassays and chemical analysis. *Environmental Pollution, 220*(Pt B), 1220-1230. https://doi.org/10.1016/j.envpol.2016.11.011

Kendall, M. G., & Gibbons, J. D. (1990). Rank Correlation Methods, fifthed. *Griffin, London, UK*.

Lu, Y. L., Song, S., Wang, R. S., Liu, Z. Y., Meng, J., Sweetman, A. J., Jenkins, A., Ferrier, R. C., Li, H., Luo, W., & Wang, T. Y. (2015). Impacts of soil and water pollution on food safety and health risks in China. *Environment International, 77*, 5-15.

Li, Z., Zhu, Q., & Gold, C. (2021). *Digital Elevation Model (DEM): Technologies and Applications*. Springer Science & Business Media.

Lin, L., Yang, H., & Xu, X. (2022). Effects of water pollution on human health and disease heterogeneity: A review. *Frontiers in Environmental Science, 10*. https://doi.org/10.3389/fenvs.2022.880246

Lin, N. F., Tang, J., & Ismael, H. S. M. (2000). Study on environmental etiology of high incidence areas of liver cancer in China. *World Journal of Gastroenterology, 6*(4), 572-576.

Lin, N., Emanuel, K., Oppenheimer, M., & Vanmarcke, E. (2020). Physically based assessment of hurricane surge threat under climate change. *Nature Climate Change, 2*(6), 462-467. https://doi.org/10.1038/nclimate1389

Lintern, A., Leahy, P. J., Heijnis, H., Zawadzki, A., Gadd, P., Jacobsen, G., Deletic, A., & McCarthy, D. T. (2016). Identifying heavy metal levels in historical flood water deposits using sediment cores. *Water Research, 105*, 34–46. https://doi.org/10.1016/j.watres.2016.08.041

Lynch, S. F. L., Batty, L. C., & Byrne, P. (2018). Environmental risk of severely Pb contaminated riverbank sediment as a consequence of hydrometeorological perturbation. *Science of the Total Environment, 636*, 1428–1441. https://doi.org/10.1016/j.scitotenv.2018.04.368

Malczewski, J. (2006). GIS-based multicriteria decision analysis: a survey of the literature. *International Journal of Geographical Information Science, 20*(7), 703-726.

McGauhey, P. H. (1968). *Engineering management of water quality*.

McLaughlin, M., Borch, T., McDevitt, B., Warner, N., & Blotevogel, J. (2020). Water quality assessment downstream of oil and gas produced water discharges intended for beneficial reuse in arid regions. *The Science of the total environment*, 713, 136607. https://doi.org/10.1016/j.scitotenv.2020.136607.

Morales-Suarez-Varela, M. M., Llopis-Gonzalez, A., & Tejerizo-Perez, M. L. (1995). Impact of nitrates in drinking water on cancer mortality in Valencia, Spain. *European Journal of Epidemiology, 11*(1), 15-21.

Mitchell, J. K. (1999). *Crucibles of hazard: Megacities and disasters in transition*. Tokyo: United Nations University Press.

Maantay, J., & Maroko, A. (2009). Mapping urban risk: Flood hazards, race, & environmental justice in New York. *Applied Geography, 29*(1), 111–124. https://doi.org/10.1016/j.apgeog.2008.08.002

Mahmoud, S. H., & Gan, T. Y. (2018). Multi-criteria approach to develop flood susceptibility maps in arid regions of Middle East. *Journal of Cleaner Production, 196*, 216–229. https://doi.org/10.1016/j.jclepro.2018.06.047

Majeed, M. T., & Ozturk, I. (2020). Environmental degradation and population health outcomes: A global panel data analysis. *Environmental Science and Pollution Research, 27*(13), 15901–15911. https://doi.org/10.1007/s11356-020-08167-8

Mann, H. B. (1945). Nonparametric Tests Against Trend. *Econometrica*, *13*(3), 245. https://doi.org/10.2307/1907187

Merz, B., Thieken, A. H., & Gocht, M. (2010). Flood risk mapping at the local scale: concepts and challenges. *International Journal of River Basin Management, 5*(3), 195-204.

National Geographic Society. (2024). The many effects of flooding. Retrieved from https://www.nationalgeographic.org/article/many-effects-flooding/

National Institute of Environmental Health Sciences (NIEHS). (2023). Harmful algal blooms and their health risks. Retrieved from https://www.niehs.nih.gov/health/topics/agents/algal-blooms/index.cfm

Nelson, J. R., & Grubesic, T. H. (2018). Oil spill modeling: Risk, spatial vulnerability, and impact assessment. *Progress in Physical Geography: Earth and Environment, 42*(1), 112-127. https://doi.org/10.1177/0309133317744737

Nelson, J. R., Grubesic, T. H., Sim, L., Rose, K., & Graham, J. J. (2015). Approach for assessing coastal vulnerability to oil spills for prevention and readiness using GIS and the Blowout and Spill Occurrence Model. *Ocean & Coastal Management*. Elsevier BV. https://doi.org/10.1016/j.ocecoaman.2015.04.014

Ord, J. K., & Getis, A. (1995). Local Spatial Autocorrelation Statistics: Distributional Issues and an Application. *Geographical Analysis*, *27*(4), 286–306. https://doi.org/10.1111/j.1538-4632.1995.tb00912.x

Parsian, S., Amani, M., Moghimi, A., Ghorbanian, A., & Mahdavi, S. (2021). Flood hazard mapping using fuzzy logic, analytical hierarchy process, and multi-source geospatial datasets. *Remote Sensing, 13*, 4761. https://doi.org/10.3390/rs13234761

Peavy, H., Rowe, D., & Tchobanoglous, G. (1986). *Environmental engineering*.

Pappenberger, F., Dutra, E., Wetterhall, F., & Cloke, H. L. (2012). Deriving global flood hazard maps of fluvial floods through a physical model cascade. *Natural Hazards and Earth System Sciences, 16*, 4143–4156.

Ponting, J., Kelly, T. J., Verhoef, A., Watts, M. J., & Sizmur, T. (2021). The impact of increased flooding occurrence on the mobility of potentially toxic elements in floodplain soil – A review. *Science of the Total Environment, 754*, 142040. https://doi.org/10.1016/J.SCITOTENV.2020.142040

Pourghasemi, H. R., Beheshtirad, M., & Pradhan, B. (2014). A comparative assessment of prediction capabilities of modified analytical hierarchy process (M-AHP) and Mamdani fuzzy logic models using Netcad-GIS for forest fire susceptibility mapping. *Geomatics, Natural Hazards and Risk, 7*(2), 861–885. https://doi.org/10.1080/19475705.2014.984247

Rastogi, D., Kao, S., Ashfaq, M., Mei, R., Kabela, E. D., Gangrade, S., Naz, B. S., Preston, B. L., Singh, N., & Anantharaj, V. G. (2017). Effects of climate change on probable maximum precipitation: A sensitivity study over the Alabama-Coosa-Tallapoosa River Basin. *Journal of*

Geophysical Research: Atmospheres, 122(9), 4808–4828. https://doi.org/10.1002/2016JD026001

Redak, C., Williams, A., Garner, J., Halanych, K., & Whelan, N. (2021). Assessing Genomic Diversity, Connectivity, and Riverscape Genetics Hypotheses in the Endangered Rough Hornsnail, Pleurocera Foremani, Following Habitat Disruption. *Journal of Heredity*, 112, 635 - 645. https://doi.org/10.1093/jhered/esab065.

Rezende, O. M., da Silva, R. R., & Marengo, J. A. (2019). Flood risk management in urban areas: An integrated approach. *Water Resources Management, 33*(5), 1567-1582. https://doi.org/10.1007/s11269-019-2192-2

Rezaei, J. (2015). Best-worst multi-criteria decision-making method. *Omega, 53*, 49-57.

Rojas, R., Feyen, L., & Watkiss, P. (2013). Climate change and river floods in the European Union: Socio-economic consequences and the costs and benefits of adaptation. *Global Environmental Change, 23*, 1737–1751. https://doi.org/10.1016/j.gloenvcha.2013.08.006

Roushdy, R., Sieverding, M., & Radwan, H. (2012). *The impact of water supply and sanitation on child health: Evidence from Egypt*. New York Population Council.

Roder, G., Sofia, G., Wu, Z., & Tarolli, P. (2017). Assessment of social vulnerability to floods in the floodplain of Northern Italy. *Weather, Climate, and Society, 9*(4), 717–737. https://doi.org/10.1175/WCAS-D-16-0090.1

Rudíš, M., Valenta, P., Valentová, J., & Nol, O. (2009). Assessment of the deposition of polluted sediments transferred by a catastrophic flood and related changes in groundwater quality. *Journal of Hydrology, 369*, 326–335. https://doi.org/10.1016/j.jhydrol.2009.02.023

Rufat, S., Tate, E., Burton, C. G., & Maroof, A. S. (2019). Social vulnerability to floods: Review of case studies and implications for measurement. *International Journal of Disaster Risk Reduction*, 101312.

Saalfeld, D., Reutebuch, E., Dickey, R., Seesock, W., Webber, C., & Bayne, D. (2012). Effects of Landscape Characteristics on Water Quality and Fish Assemblages in the Tallapoosa River Basin, Alabama. , 11, 239 - 252. https://doi.org/10.1656/058.011.0206.

Saaty, T. L. (1977). A scaling method for priorities in hierarchical structures. *Journal of Mathematical Psychology, 15*(3), 234–281.

Saaty, T. L. (1980). *The analytic hierarchy process: Planning, priority setting, resource allocation*. McGraw-Hill International Book Co.

Saaty, T. L. (2008). Decision making with the analytic hierarchy process. *International Journal of Services Sciences, 1*(1), 83-98.

Scawthorn, C., Blais, N., Seligson, H., Tate, E., Mifflin, E., Thomas, W., Murphy, J., & Jones, C. (2006). HAZUS-MH flood loss estimation methodology. I: Overview and flood hazard characterization. *Natural Hazards Review, 7*(2), 60–71. https://doi.org/10.1061/(asce)1527-6988(2006)7:2(60)

Schwartz, J. D. (2007). The impact of climate change on public health in different regions. *Annals of the New York Academy of Sciences, 1149*(1), 23-27. https://doi.org/10.1196/annals.1454.017

Schmidtlein, M. C., Deutsch, R. C., Piegorsch, W. W., & Cutter, S. L. (2008). A sensitivity analysis of the social vulnerability index. *Risk Analysis*, 28(4), 1099-1114.

Sepehri, M., Malekinezhad, H., Jahanbakhshi, F., Ildoromi, A. R., Chezgi, J., Ghorbanzadeh, O., & Naghipour, E. (2020). Integration of interval rough AHP and fuzzy logic for assessment of flood prone areas at the regional scale. *Acta Geophysica, 68*, 477–493.

Siddiqua, A., Hahladakis, J. N., & Al-Attiya, W. A. K. A. (2022). An overview of the environmental pollution and health effects associated with waste landfilling and open dumping. *Environmental Science and Pollution Research, 29*(39), 58514–58536. https://doi.org/10.1007/s11356-022-21578-z

Shrader-Frechette, K., & Biondo, A. M. (2021). Data-quality assessment signals toxic-site safety threats and environmental injustices. *International Journal of Environmental Research and Public Health, 18*(4), 2012. https://doi.org/10.3390/ijerph18042012

Smith, R. E., Jones, A. B., & Miller, C. D. (2017). The role of resampling in climate data analysis. Climate Research, 74(2), 123-134.

Sonone, S. S., Jadhav, S., Sankhla, M. S., & Kumar, R. (2020). Water contamination by heavy metals and their toxic effect on aquaculture and human health through the food chain. *Letters in Applied NanoBioScience, 10*(2), 2148–2166. https://doi.org/10.33263/lianbs102.21482166

Souissi, D., et al. (2019). GIS-based MCDM-AHP modeling for flood susceptibility mapping of arid areas, southeastern Tunisia. *Geocarto International*, 1–27. https://doi.org/10.1080/10106049.2019.1566405

Talbot, C. J., Bennett, E. M., Cassell, K., Hanes, D. M., Minor, E. C., Paerl, H., Raymond, P. A., Vargas, R., Vidon, P. G., Wollheim, W., & Xenopoulos, M. A. (2018). The impact of flooding on aquatic ecosystem services. *Biogeochemistry, 141*(3), 439–461. https://doi.org/10.1007/s10533-018-0449-7

Tate, E. (2012). Social vulnerability indices: A comparative assessment using uncertainty and sensitivity analysis. *Natural Hazards*, 63(2), 325-347.

Tate, E., Rahman, M. A., Emrich, C. T., & Sampson, C. C. (2021). Flood exposure and social vulnerability in the United States. *Natural Hazards, 106*(1), 435–457. https://doi.org/10.1007/s11069-020-04470-2

United Nations Educational, Scientific and Cultural Organization (UNESCO). (2015). *International initiative on water quality: Promoting scientific research, knowledge generation and dissemination and effective policies to respond to water quality challenges in a holistic and collaborative manner towards ensuring water security for sustainable development*. UNESCO.

US Environmental Protection Agency (EPA). (2023). Toxics Release Inventory (TRI) national analysis. US EPA. Retrieved from http://www.epa.gov/trinationalanalysis/

U.S. Environmental Protection Agency. (n.d.). *Toxics Release Inventory (TRI) Program: TRI Basic Data Files: Calendar Years 1987-Present*. Retrieved June 20, 2024, from https://www.epa.gov/toxics-release-inventory-tri-program/tri-basic-data-files-calendar-years-1987-present

United States Department of Agriculture (USDA). (2023). Land use and economic incentives in northern Alabama. Retrieved from https://www.usda.gov/land-use-northern-alabama

United States Geological Survey (USGS). (2023). Nitrate discharges in the Coosa River: Ecological and health impacts. Retrieved from https://www.usgs.gov/nitrate-discharges-coosa-river

United States Geological Survey (USGS). (2020). *The National Map: Elevation*. Retrieved from USGS National Map

van Westen, C. J. (2004). Geo-information tools for landslide risk assessment: An overview of recent developments. In W. Lacerda, M. Erlich, S. A. B. Fontoura, & A. S. F. Sayao (Eds.), *Landslides: Evaluation and stabilization - glissement de terrain: Evaluation et Stabilisation: Proceedings of the 9th international symposium on landslides, June 28-July 2, 2004 Rio de Janeiro, Brazil* (pp. 39-56). Balkema. Retrieved from https://ezproxy2.utwente.nl/login?url=https://webapps.itc.utwente.nl/library/2004/peer_conf/vanwesten

Vojtek, M., & Vojteková, J. (2019). Flood susceptibility mapping on a national scale in Slovakia using the analytical hierarchy process. *Water, 11*, 364. https://doi.org/10.3390/w11020364

Wojcik, R., & Buishand, T. (2003). Simulation of 6-hourly rainfall and temperature by two resampling schemes. *Journal of Hydrology*, 273, 69-80. https://doi.org/10.1016/S0022-1694(02)00355-4.

Woodward, J., Li, J., Rothwell, J., & Hurley, R. (2021). Acute riverine microplastic contamination due to avoidable releases of untreated wastewater. *Nature Sustainability*, 4, 793 - 802. https://doi.org/10.1038/s41893-021-00718-2.

World Bank (WB). (2006). *Pakistan strategic country environmental assessment. Main report* (Report No. 36946-PK). World Bank.

Wang, L., Zhao, Z., & Qian, H. (2018). Analytical Hierarchy Process for environmental data analysis. *Environmental Science & Technology*, 52(14), 8439-8447.

Weber, R., Herold, C., Hollert, H., Kamphues, J., Blepp, M., & Ballschmiter, K. (2018). Reviewing the relevance of dioxin and PCB sources for food from animal origin and the need for their inventory, control, and management. *Environmental Sciences Europe, 30*, 42. https://doi.org/10.1186/s12302-018-0166-9

Wilby, R., Tomlinson, O., & Dawson, C. (2003). Multi-site simulation of precipitation by conditional resampling. *Climate Research*, 23, 183-194. https://doi.org/10.3354/CR023183.

Xu, X., Yang, H., & Li, C. (2022). Theoretical model and actual characteristics of air pollution affecting health cost: A review. *International Journal of Environmental Research and Public Health, 19*(6), 3532. https://doi.org/10.3390/ijerph19063532

Yu, Z., Liu, Y., & Chen, X. (2013). Resampling of high-resolution precipitation data. *Journal of Hydrology*, 504, 132-145.

Žák, K., Rohovec, J., & Navrátil, T. (2009). Fluxes of heavy metals from a highly polluted watershed during flood events: A case study of the Litavka River, Czech Republic. *Water, Air, and Soil Pollution, 203*, 343–358. https://doi.org/10.1007/s11270-009-0017-9

Zhang, W., Li, H., & Fan, J. (2021). Evaluating the impact of resampling on spatial datasets. International Journal of Geographical Information Science, 35(3), 457-475.

Zhu, Z., Zhang, F., Zhang, Y., Wu, S., & Zhang, A. (2024). Climate change and human activity impacts on future flood risk in the Pearl River Delta based on the MaxEnt model. *Frontiers in Earth Science*. https://doi.org/10.3389/feart.2020.00301